the plant journal

SEB SOCIETY FOR EXPERIMENTAL BIOLOGY

The Plant Journal (2024) **119,** 1112–1133 doi: 10.1111/tpj.16765

RESOURCE

Integrating multi-omics data reveals energy and stress signaling activated by abscisic acid in Arabidopsis

Takuya Yoshida[1,2,*,†,‡], Julia Mergner[3,4], Zhenyu Yang[1], Jinghui Liu[1], Bernhard Kuster[4], Alisdair R. Fernie[2] and Erwin Grill[1,*]

[1]*Lehrstuhl für Botanik, Technische Universität München, Emil-Ramann-Str. 4, 85354 Freising, Germany, and*
[2]*Max-Planck-Institut für Molekulare Pflanzenphysiologie, 14476 Potsdam-Golm, Germany,*
[3]*Bavarian Center for Biomolecular Mass Spectrometry at Klinikum rechts der Isar (BayBioMS@MRI), Technical University of Munich, Munich, Germany,*
[4]*Chair of Proteomics and Bioanalytics, Technical University of Munich, Freising, Germany*

Received 8 July 2023; revised 24 March 2024; accepted 31 March 2024; published online 13 April 2024.
*For correspondence (e-mail erwin.grill@tum.de; takuya.yoshida@tum.de).
†Present address: Trans-Omics Facility, National Institute for Basic Biology, 444-8585, Okazaki, Japan
‡Present address: Basic Biology Program, The Graduate University for Advanced Studies, SOKENDAI, 444-8585, Okazaki, Japan

SUMMARY

Phytohormones are essential signaling molecules regulating various processes in growth, development, and stress responses. Genetic and molecular studies, especially using *Arabidopsis thaliana* (Arabidopsis), have discovered many important players involved in hormone perception, signal transduction, transport, and metabolism. Phytohormone signaling pathways are extensively interconnected with other endogenous and environmental stimuli. However, our knowledge of the huge and complex molecular network governed by a hormone remains limited. Here we report a global overview of downstream events of an abscisic acid (ABA) receptor, REGULATORY COMPONENTS OF ABA RECEPTOR (RCAR) 6 (also known as PYRABACTIN RESISTANCE 1 [PYR1]-LIKE [PYL] 12), by integrating phosphoproteomic, proteomic and metabolite profiles. Our data suggest that the RCAR6 overexpression constitutively decreases the protein levels of its coreceptors, namely clade A protein phosphatases of type 2C, and activates sucrose non-fermenting-1 (SNF1)-related protein kinase 1 (SnRK1) and SnRK2, the central regulators of energy and ABA signaling pathways. Furthermore, several enzymes in sugar metabolism were differentially phosphorylated and expressed in the RCAR6 line, and the metabolite profile revealed altered accumulations of several organic acids and amino acids. These results indicate that energy- and water-saving mechanisms mediated by the SnRK1 and SnRK2 kinases, respectively, are under the control of the ABA receptor-coreceptor complexes.

Keywords: abscisic acid, phosphoproteomics, proteomics, metabolite profiling, *Arabidopsis thaliana*, receptor, kinase, energy signaling, stress response.

INTRODUCTION

Phytohormones are vital signaling molecules mediating endogenous and environmental cues and are involved in various processes of growth, development, and stress responses. Upon phytohormone perception, their signaling pathways, including gene expression, are activated. Extensive genetic and molecular studies, especially using the model plant *Arabidopsis thaliana* (Arabidopsis), have revealed the core signaling components of classical phytohormones (Lumba et al., 2010). However, although the central regulators play critical roles in phytohormone responses, the signaling pathways are heavily interconnected with other phytohormones and signals. For instance, phytohormone signals were shown to be extensively integrated via protein–protein interaction (PPI) (Altmann et al., 2020). Furthermore, endogenous and environmental stimuli, such as sugars and light, are also associated with phytohormone signaling pathways (de Wit et al., 2016; Ljung et al., 2015). Therefore, our knowledge about the large and complex molecular network governed by a phytohormone remains limited.

The phytohormone abscisic acid (ABA) accumulates in response to cellular water deficit during seed maturation

and under abiotic stress conditions, such as drought. According to the current model, ABA signal transduction starts from its perception by the cytosolic receptors, designated as REGULATORY COMPONENTS OF ABA RECEPTOR (RCAR), PYRABACTIN RESISTANCE1 (PYR1), or PYR1-LIKE (PYL), and coreceptors, clade A protein phosphatases of type 2C (PP2C) (Ma et al., 2009; Park et al., 2009). The formation of the receptor-coreceptor complex leads to the activation of subclass III sucrose-nonfermenting-1 (SNF1)-related kinase 2s (SnRK2s). Then, the activated SnRK2s regulate substrate transcription factors and membrane channels via phosphorylation, resulting in stress-responsive gene expression and stomatal closure (Cutler et al., 2010; Raghavendra et al., 2010). As evidenced by its extreme ABA-insensitive phenotypes of the triple *snrk2* Arabidopsis mutant, three subclass III SnRK2s are pivotal activators of ABA signaling, and transcriptome and phosphoproteome analyses using the *snrk2* mutant revealed their downstream genes (Fujii & Zhu, 2009; Fujita et al., 2009) and candidate phosphorylation substrates (Umezawa et al., 2013; Wang et al., 2013). ABA signal transduction was supposed to be nearly completely blocked in the triple *snrk2* mutant, and exogenous ABA application was employed in these studies to reveal the SnRK2-meditated pathways in ABA signaling. By contrast, the triple mutants of the PP2Cs showed enhanced ABA sensitivity and increased expression of ABA-inducible genes (Rubio et al., 2009). However, experimental evidence on the molecular events turned on by endogenous ABA is lacking, especially besides transcriptomic changes.

There are 14 RCARs in Arabidopsis, and all were demonstrated to be functional ABA receptors interacting with clade A PP2Cs (Tischer et al., 2017). The RCARs are thought to have overlapping functions as the clearer phenotypes of multiple knockout mutants (Gonzalez-Guzman et al., 2012; Park et al., 2009; Zhao et al., 2018) indicated, while gene-specific roles were also suggested. For instance, the ectopic expression of RCAR1 (also known as PLY9) under a stress-inducible promoter enhanced drought stress resistance and leaf senescence, suggesting a distinct role of RCAR1 in these responses (Zhao, Chan, et al., 2016). Previously, we also examined the growth characteristic of the overexpressing lines of 14 RCARs, and the lines of several RCARs, including RCAR1, RCAR6 (also known as PYL12), and RCAR10 (also known as PYL4), showed increased leaf temperature without apparent growth retardation (Yang et al., 2016). Further analyses suggested that the RCAR6 line was water productive, i.e., exhibited an increased water use efficiency (WUE) with high growth rates, most likely because of the maintenance of net carbon assimilation rate by compensatory increases of leaf CO_2 gradients. However, molecular explanations behind the growth phenotypes in the RCAR lines are not fully understood.

Nowadays, comprehensive quantifications of transcripts, proteins, protein posttranslational modifications, and metabolites are powerful and versatile tools for investigating molecular processes. These large-scale data are valuable and informative, and additionally, integrative analyses are important to address how the different layers of molecular organization are associated. Here we performed multi-omics analyses, including proteomic, phosphoproteomic, and metabolite profiling, to obtain an overview of the signaling network regulated by RCAR ABA receptors. The phosphoproteomic and proteomic profiles showed that the RCAR6 overexpression resulted in the activation of SnRK1 and SnRK2 kinases and the decreased proteins of the PP2C coreceptor. In addition, the RCAR6 line also showed an altered metabolite profile, including decreased levels of several organic acids and amino acids. These omics profiles were further integrated with available data on PPI and metabolic pathways, providing insights into molecular mechanisms underlying water-productive phenotypes of the RCAR6 line.

RESULTS

Hundreds of phosphopeptides were differentially phosphorylated on RCAR6 overexpression

Upon the perception of ABA molecules by the RCAR receptors and their coreceptors, clade A PP2C phosphatases, the PP2Cs are inactivated, and subsequently, the activation of SnRK2 kinases occurs (Cutler et al., 2010; Raghavendra et al., 2010). The PP2Cs were also reported to dephosphorylate several kinases, including the SnRK1s and calcineurin B-like protein (CBL)-interacting protein kinase 23 (CIPK23) (Léran et al., 2015; Rodrigues et al., 2013). To investigate molecular events by the inactivation of PP2Cs, we performed phosphoproteomic analyses using the RCAR overexpressing lines (Yang et al., 2016, 2019). The wild type (Col-0) and the overexpressing lines were grown under short-day and well-watered or moderate water scarcity conditions, and leaf materials were harvested (Figure S1). The numbers of biological replicates of protein extracts for phosphoproteomic and proteomic analyses were three (Col-0), four (RCAR6), and two (RCAR10) under control conditions, while those of each line were three under drought stress conditions (Figure S1c). The two biological replicates for the RCAR10 line under control conditions were considered insufficient for statistical analyses, and therefore, we hereafter mainly described and discussed the results from the RCAR6 line. Protein extracts from leaf tissues were labeled by tandem mass tags (TMT), phosphopeptide fractions were enriched, and nanoflow liquid chromatography coupled to tandem mass spectrometry (LC–MS/MS) was performed (Mergner et al., 2020). The control and drought stress TMT experiments were analyzed separately to identify differences among the

genotypes under either control or drought stress conditions. For a comparison between control and drought stress conditions within one genotype, these two TMT experiments were first row-wise normalized for subsequent analyses. In total, 8790 phosphosites (class I; localization probability >0.75) were identified by these two TMT multiplexing experiments (Data S1a,b), and 4860 phosphosites, which were detected and quantified in both TMT experiments (Data S1c), were further comparatively analyzed between the two conditions (Figure S2). Principal component analysis (PCA) showed that the phosphosites varied under the two conditions, and the number of differentially phosphorylated phosphosites among these three lines under control conditions was higher than that under drought stress conditions (Figure S2b,c). Moreover, the phosphorylation of 192 and 25 phosphosites (corresponding to 162 and 22 proteins) was shown to be increased and decreased, respectively, in the RCAR6 line compared to wild type (Figure 1a,b; Figure S2d–f; Table S1). Ten phosphosites were differentially phosphorylated under control and drought stress conditions (Figure S2c), and only two proteins, SUCROSE PHOSPHATE SYNTHASE (SPS) 4F (AT4G10120.3) and INCREASE IN BONSAI METHYLATION (IBM) 1 (AT3G07610.1), were significantly more highly phosphorylated in the RCAR6 line under both conditions. The phosphorylation of the same Ser180 of SPS4F was increased in the RCAR6 line under both conditions, while the Ser895 and Ser99 of IBM1 were highly phosphorylated under control and drought stress conditions, respectively.

Furthermore, a number of peptides were differentially phosphorylated in both RCAR6 and RCAR10 lines. While 180 and 11 phosphopeptides increased in the RCAR6 line under control and drought stress conditions, respectively, 45 and one phosphopeptides also exhibited increased phosphorylation in the RCAR10 line (Table S1). By contrast, among 18 and seven decreased phosphopeptides in the RCAR6 line under control and drought stress conditions, respectively, 12 and one phosphopeptides also decreased in the RCAR10 line. In sum, 46 and 13 phosphosites were increased and decreased in both RCAR lines, and these phosphosites might include their common downstream targets.

SnRK2 and SnRK1 were activated in the RCAR6 overexpressing line

To obtain insights into the differentially phosphorylated proteins on RCAR6 overexpression, Gene Ontology (GO) analyses were performed. While no enriched GO terms were found in the less phosphorylated proteins in the RCAR6 line, the proteins associated with the GO terms "Protein phosphorylation," "Alternative mRNA splicing," and "Chloroplast relocation" were enriched in the highly phosphorylated proteins (Figure 1c). There were 23 proteins grouped into "Protein phosphorylation" (Table S2) and the phosphopeptides corresponding to SRK2D (also known as SnRK2.2) and KIN10, KIN11, or KIN12 (also known as SnRK1.1, SnRK1.2 or SnRK1.3) were significantly increased in the RCAR6 line under control conditions (Figure 1d). Notably, the Ser177 of SRK2D was the corresponding residue in the activation loop, which was crucial for the kinase activity and dephosphorylated by the PP2Cs (Belin et al., 2006; Boudsocq et al., 2007; Vlad et al., 2009) (Figure S3a). Also, the Thr175 of KIN10 has been well studied as the T-loop, which requires phosphorylation for the kinase activity and is conserved in eukaryotes (Baena-González et al., 2007; Estruch et al., 1992; Hawley et al., 1996) (Figure S3b). Venn diagrams were further depicted to evaluate how many possible substates of SnRK2 or SnRK1 kinases (Nukarinen et al., 2016; Umezawa et al., 2013; Wang et al., 2013) were found in our data (Figure S3c,d; Table S3). In addition to SRK2D, the DEK-domain-containing protein DEK3, which was involved in modulating chromatin structure (Waidmann et al., 2014), was differentially phosphorylated in both SnRK2 phosphoproteomic studies, and nine more reported substrates were differentially phosphorylated in the RCAR6 line (Figure S3c, e; Table S3). Moreover, the phosphorylation of seven reported substrates of the SnRK1 kinase was increased or decreased in the RCAR6 line (Figure S3d,f; Table S3). Motifs representing amino acid preferences flanking the phosphorylation sites were searched in these phosphopeptides. However, no motifs were found to be enriched. While the increased phosphorylation of SRK2D but not that of KIN10, KIN11, or KIN12 was clear in the RCAR10 line (Figure 1d), six of their substrates, including DEK3, were also differentially phosphorylated in the RCAR10 line (Table S3). Taken together, these results suggest that the SnRK2 and SnRK1 kinases and their downstream pathways were activated by the RCAR6 overexpression.

In addition to SnRK2 and SnRK1 kinases, other kinases, including mitogen-activated protein kinase kinase kinases (MAPKKKs), CIPK9 (also known as SnRK3.12), and receptor-like kinases (RLKs), were highly phosphorylated in the RCAR6 line (Table S2). Notably, the Thr178 of CIPK9, which corresponds to one of the crucial phosphosites of CIPK24 (also known as SOS2) in the activation loop (Gong et al., 2002), was highly phosphorylated in the RCAR6 line (Figure S4a,c). Given that the SP motif was found to be enriched (Figure S2f) being a common target of several families of kinases including SnRK2s and RLKs (van Wijk et al., 2014), our results implied that several kinase signaling pathways were broadly affected by the RCAR6 overexpression. This view was also supported by the partial overlap with the possible substrates of the SnRK2 and SnRK1 kinases (Nukarinen et al., 2016; Umezawa et al., 2013; Wang et al., 2013) (Figure S3; Table S3).

The enriched GO term "Chloroplast relocation" consisted of six proteins (Table S4), including two blue-light

receptor kinases, PHOTOTROPIN 1 (PHOT1) and PHOT2, which were included under the GO term "Protein phosphorylation". Notably, the conserved serine in the hinge region between two light, oxygen, voltage domains were highly phosphorylated in the RCAR6 line (Figure S4b,d). Moreover, 12 phosphopeptides of eight proteins in the GO term "Alternative mRNA splicing" were increased in the RCAR6 line (Table S5). In addition to the zinc finger protein SERRATE (SE), a potential substrate of the SnRK2s (Yan et al., 2017), six serine/arginine-rich (SR) proteins were highly phosphorylated in the RCAR6 line. These results suggested that the processes regulated via the blue light signaling and mRNA splicing were altered in the RCAR6 line.

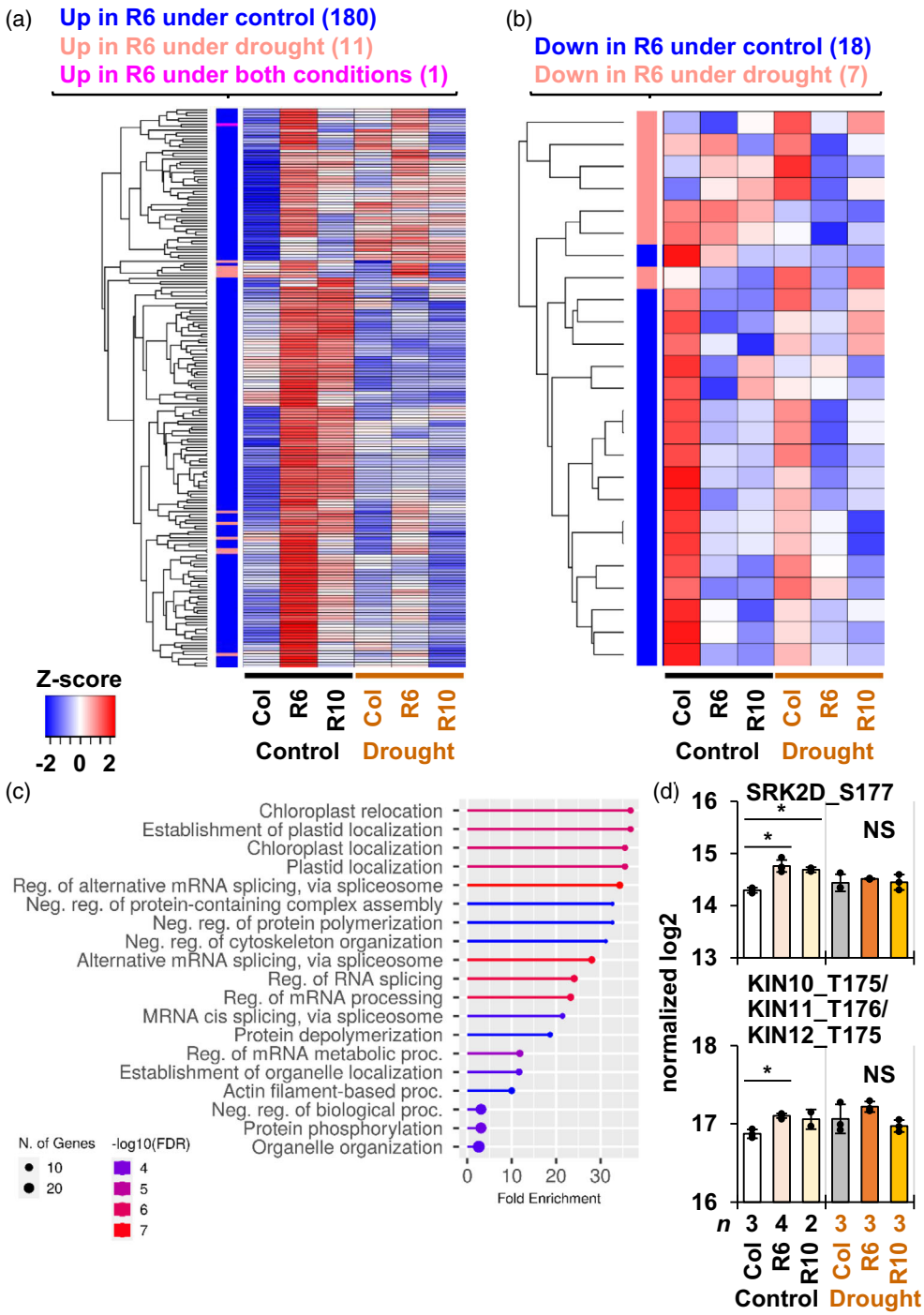

Figure 1. Differentially phosphorylated proteins in the RCAR overexpressing lines.
A phosphoproteome analysis for protein samples extracted from leaf materials of Col-0, RCAR6-ox (R6) and RCAR10-ox (R10) lines was performed by liquid chromatography coupled to tandem mass spectrometry as described previously (Mergner et al., 2020). Protein identification was performed using the MaxQuant software (version 1.5.8.3), and the intensities of tandem mass tag (TMT) labelling were analyzed using the Perseus software (version 1.5.5.3).
(a, b) Heat maps showing significantly (*posthoc* false discovery rate [FDR] <0.01) increased (a) and decreased (b) abundant phosphosites in the R6 line compared to Col-0 under control and drought stress conditions. The numbers of phosphosites are shown in parentheses.
(c) Significantly enriched Gene Ontology (GO) terms in the phosphopeptides increased in the R6 line. The enriched (FDR <0.05) GO Biological Processes were identified using the ShinyGO tool (version 0.77). No enriched GO terms were found in the phosphopeptides decreased in the R6 line.
(d) The row-wise normalized log2 intensities of the SRK2D (S177) and KIN10 (T175)/KIN11 (T176)/KIN12 (T175) phosphosites. The latter was identified by a peptide mapping to KIN10, KIN11 and KIN12. Bar graphs with error bars indicate mean ± SD, and dots represent the raw data ($n = 2$–4). Asterisks denote statistically significant differences ($P < 0.01$) by single-factor ANOVA among three lines, and no marks represent no differences. NS states there are no significant differences among the three lines.

Different phosphosites were altered by RCAR6 overexpression and drought stress

The phosphoproteomic data were further analyzed to identify drought stress-responsive phosphopeptides (Figure S5). Among 89 phosphopeptides differentially (false discovery rate [FDR] <0.05) phosphorylated in wild type under control and drought stress conditions, 40 and 49 phosphopeptides were increased and decreased in response to drought stress. These 89 phosphosites were subsequently considered drought stress-responsive phosphosites. By contrast, over 600 phosphopeptides were differentially phosphorylated in the RCAR6 line under control and drought stress conditions. This result might be reflected by an increased number of phosphopeptides differentially phosphorylated under control conditions (Figure S2c). The increased and decreased abundance of phosphosites under drought stress conditions appeared to be similar in target amino acids and motifs (Figure S5c–e). Moreover, the proteins grouped into GO terms associated with mRNA processing were enriched in increased and decreased abundant phosphosites (Figure S6). However, the drought stress-responsive phosphosites slightly overlapped with those differentially phosphorylated sites in the RCAR6 line (Figure S6c). Collectively, these results suggest that RCAR6 overexpression and drought stress might stimulate the same processes, including mRNA processing, via different phosphorylation pathways.

The RCAR6 overexpression decreased the protein levels of PP2Cs

To obtain insights into proteomic changes by the overexpression of RCARs, we performed a full proteomic analysis using TMT-based quantification (Mergner et al., 2020). The protein samples and the numbers of biological replicates were exactly the same as the phosphoproteomic analysis (Figure S1c). Thus, as in the phosphoproteome result sections, we hereafter mainly described and discussed the results from the RCAR6 line. Afte the TMT labeling, the flow-through fractions of phosphopeptide enrichment were analyzed using LC–MS/MS. In total, 11 082 proteins were quantified (Data S1d,e), and 9833 proteins (Data S1f) were further analyzed as validly and reproducibly identified proteins (Figure S7). PCA revealed that these protein profiles varied under two conditions, and the differentially accumulated proteins among these three lines slightly overlapped (Figure S7b,c). In addition, the protein levels of the overexpressed RCARs were verified, whilst we observed variations to some extent among the samples under drought stress conditions (Figure S7d). Compared to the proteomic profile of wild type, 155 and 183 proteins were increased and decreased in the RCAR6 overexpressing line (Figure 2; Table S6). Like the phosphoproteomic changes, where only one phosphopeptide was altered under both control and drought stress conditions, 2 and 10 proteins were increased or decreased in the RCAR6 line under both conditions. Interestingly, several RCAR receptors and PP2C coreceptors exhibited alterations in protein levels. The protein levels of RCAR11 (also known as PYR1) and HOMOLOGY TO ABA INSENSITIVE (ABI) 2 (HAB2), a clade A PP2C, were significantly decreased in the RCAR6 line under both control and drought stress conditions (Figure 2c; Figure S7e). Furthermore, RCAR1 (and RCAR2, also known as PYL7) and two PP2Cs, ABI1 and ABI2, also showed apparent decreases in the RCAR6 line under either condition. Given that the RCAR overexpression enhanced the sensitivity to ABA during seed germination (Yang et al., 2016), the increased sensitivity to ABA might be caused by the decreased protein levels of PP2Cs, as the *pp2c* knockout mutants were hypersensitive to ABA (Rubio et al., 2009). By contrast, ABA signaling in the RCAR lines might also be dampened to some extent via the decreased levels of other RCARs, possibly due to negative feedback regulation.

The differentially expressed proteins in both RCAR lines were further explored (Table S6). While 124 and 29 proteins increased in the RCAR6 line under control and drought stress conditions, respectively, 36 and nine proteins also increased in the RCAR10 line. In addition, the peptide mapped to glycoside hydrolases (AT3G18070 and AT3G18080) increased in the RCAR6 line under both conditions and the RCAR10 line under drought stress conditions. By contrast, 126 and 47 proteins decreased in the RCAR6 line under control and drought stress conditions,

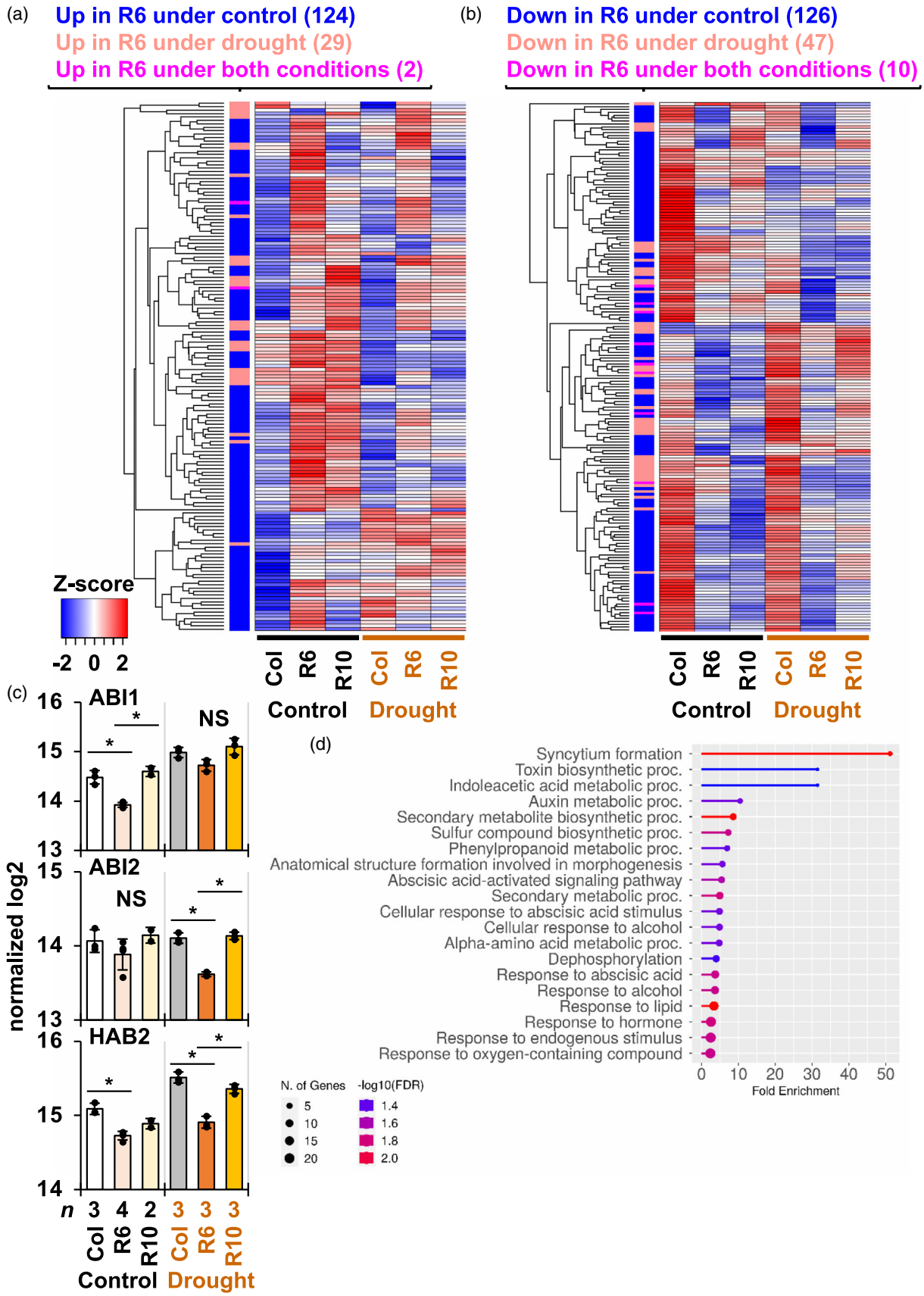

Figure 2. Differentially expressed proteins in the RCAR overexpressing lines.
A full proteome analysis for protein samples extracted from leaf materials of Col-0, RCAR6-ox (R6) and RCAR10-ox (R10) lines was performed described previously (Mergner et al., 2020). Protein identification was performed using the MaxQuant software (version 1.5.8.3), and the intensities of tandem mass tag (TMT) labelling were analyzed using the Perseus software (version 1.5.5.3).
(a, b) Heat maps showing significantly (*posthoc* false discovery rate [FDR] <0.01) increased (a) and decreased (b) proteins in the R6 line compared to Col-0 under control and drought stress conditions. The numbers of proteins are shown in parentheses.
(c) The row-wise normalized log2 intensities of the PP2C peptides. Bar graphs with error bars indicate mean $\pm$ SD, and dots represent the raw data ($n = 2$–4). Asterisks denote statistically significant differences ($P < 0.01$) by single-factor ANOVA among three lines, and no marks represent no differences. NS states there are no significant differences among the three lines.
(d) Significantly enriched Gene Ontology (GO) terms in the decreased peptides in the R6 line under control conditions. The enriched (FDR <0.05) GO Biological Processes were identified using the ShinyGO tool (version 0.77).

respectively. Among them, 63 and 20 proteins also decreased in the RCAR10 line. Additionally, 6 out of 10 decreased proteins in the RCAR6 line under both conditions exhibited decreased protein levels in the RCAR10 line, at least under control conditions. In total, 46 and 89 proteins were increased and decreased in both RCAR lines, and these proteins might include their common downstream targets.

Expansins and the proteins in auxin and glucosinolate metabolism were altered by the RCAR6 overexpression

Gene Ontology analyses were further performed to examine whether specific groups of proteins were altered in the RCAR6 line. While no GO Biological Processes were found to be enriched among the increased proteins in the RCAR6 line under control conditions, the proteins involved in wax biosynthetic processes, namely SUPERKILLER 3 (SKI3) and WAX2 (also known as CER3), were enriched in those under drought stress conditions (Figure S8a,b). By contrast, 20 GO terms, such as "Syncytium formation," "Secondary metabolite biosynthetic processes," and "Response to lipid," were enriched in the decreased proteins in the RCAR6 line under control conditions (Figure 2d). Expansins are primarily included in the GO term "Syncytium formation," and several EXPANSIN A proteins, EXPA1, EXPA3, EXPA8, and EXPA11, were significantly decreased in the RCAR6 line (Figure S8c). Two out of these four expansin proteins, EXPA1 and EXPA8, were also decreased in the RCAR10 line under control conditions. These results implied that cell growth was affected in the RCAR6 and RCAR10 lines even under well-watered conditions.

The proteins classified into the GO term "Response to lipid" included ABA receptor and coreceptor proteins, including RCAR1, RCAR11, ABI1, and HAB2, and expansins, including EXPA1 and EXPA3. In addition, LIPOXYGENASE 3 (LOX3) and 1-AMINOCYCLOPROPANE-1-CARBOXYLIC ACID (ACC) OXIDASE 2 (ACO2), which are involved in jasmonic acid (JA) and ethylene biosynthesis, respectively, were shown to be decreased in the RCAR6 line. However, other proteins in these metabolic pathways were unaltered in the RCAR6 line; thus these phytohormones were unlikely to be affected at the metabolite level. By contrast, the GO analysis showed that the proteins involved in auxin metabolic processes were enriched in the decreased proteins in the RCAR6 line as well as those in secondary and sulfur metabolism (Figure 2d). Given that the tryptophan-dependent indole-3-acetic acid (IAA) biosynthetic pathway is associated with those of secondary metabolites and sulfur compounds, especially in Brassicaceae plants (Mano & Nemoto, 2012; Mitreiter & Gigolashvili, 2021; Zhao, 2018), we further explored the proteomic changes in these pathways (Figure S9). A cytochrome P450 monooxygenase (CYP79B3), an Arabidopsis aldehyde oxidase (AAO1) and a nitrilase (NIT1) in the IAA biosynthesis from tryptophan were significantly decreased in the RCAR6 line under control conditions, while a type 2 tryptophan synthase β subunit (TSB) were decreased under drought stress conditions. The protein levels of an adenosine-5′-phosphosulfate (APS) kinase (APK2) and a serine acetyltransferase (SERAT2;2) in sulfur assimilation were also decreased in the RCAR6 line. In addition, a γ-glutamyl peptidase (GGP1) and a sulfotransferase (SOT18) involved in the formation of GSL core structure were decreased in the RCAR6 line, while four enzymes involved in the modification of GSLs were increased or decreased. Collectively, these results suggested that the auxin and GSL biosynthetic pathways were altered by the RCAR6 overexpression.

The RCAR6 overexpression and drought stress altered proteomic profiles differently

The proteomic data were further analyzed to discover drought stress-responsive proteins (Figure S10). In wild type, 690 proteins were differentially (FDR <0.05) expressed under control and drought stress conditions, while over 1500 peptides were differentially expressed in the RCAR6 line. These 290 and 400 proteins increased and decreased, respectively, in response to drought in wild type were hereafter considered drought stress-responsive proteins. Following GO analyses showed that the proteins associated with transcription initiation and stomatal movement were enriched in the proteins increased under drought stress conditions (Figure S10c). However, no enriched GO terms were found among the proteins increased in the RCAR6 line under control conditions. By contrast, the proteins associated with sulfur assimilation, serine metabolism, and dephosphorylation were enriched

in proteins decreased in response to drought stress (Figure S10d). Interestingly, two APS reductases (APRs), APR1 and APR3, which produce sulfites (SO_3^{2-}) from APS (Figure S9c), were decreased in wild type under drought stress conditions, implying that sulfur assimilation was negatively regulated in response to ABA signaling and drought stress. To examine whether the proteomic changes by the RCAR6 overexpression were associated with the responses to drought stress, the differentially expressed proteins were compared (Figure S10e,f). These comparisons showed that the changes by the RCAR6 overexpression were unlikely to be similar to those under drought stress conditions. This notion appeared to be consistent with the results of GO analyses showing that different groups of proteins were enriched in the differentially expressed proteins (Figure 2d; Figures S8a and S10c,d). As exemplified by the profile of HAB2, which was increased under drought stress conditions but decreased in the RCAR6 line (Figure 2d), ABA signaling might be differently manipulated by drought stress and the RCAR6 overexpression.

Metabolite profiles of the RCAR overexpressing lines

The Arabidopsis overexpressing RCAR6 or RCAR10 lines previously showed enhanced WUE with no or minor growth trade-offs (Yang et al., 2016). Furthermore, the increased water productivity was suggested to be associated with the maintenance of net carbon assimilation rate by compensatory increases of leaf CO_2 gradients. To investigate whether the altered growth traits, including the increased leaf CO_2 gradients, are linked to changes in their primary metabolism, we analyzed metabolite profiles in the RCAR6 and RCAR10 lines by gas-chromatography mass-spectrometry (GC–MS). Leaf materials were harvested at five time points from plants grown on soil under short-day and well-watered conditions (Figure S1). In addition, watering was withheld to harvest the materials under drought stress conditions. The numbers of biological replicates for metabolite profiling were five to seven (Figure S1c). Chromatograms and mass spectra were evaluated using Chroma TOF 1.0 (LECO) and TagFinder 4.0 (Luedemann et al., 2008), resulting in the annotation of 38 primary metabolites. PCA subsequently separated the profiles roughly by genotypes (PC1) and time point (PC2) (Figure S11), indicating that the RCAR lines showed altered metabolite profiles compared to wild type. The top 20 metabolites contributing to PC1 and PC2 included sugars, sugar alcohols, amino acids, and organic acids (Figure S11b).

To obtain insights into the metabolite profiles of the RCAR lines, hierarchical clustering was performed (Figure 3). The profile of the RCAR6 line was clustered next to that of wild type at each time point, while those of the RCAR10 line were clustered together (Figure 3a). Given that the profiles were practically separated by time points (Figure S11a), statistical analyses were performed among these three genotypes in each harvesting group (Figure 3b). Several sugars and sugar alcohols, such as glucose, trehalose, and xylose, were more accumulated in the RCAR10 line, implying that the profiles of the RCAR10 line were separately clustered because of these metabolites. By contrast, although the RCAR6 line showed comparable profiles with wild type, several organic acids, such as succinate, nicotinate, and glycerate, were altered in the RCAR6 and RCAR10 lines.

Given that the RCAR lines were reported to show an increased WUE (Yang et al., 2016), we hypothesized that these lines showed altered metabolic responses under drought stress conditions. However, the profiles under control and drought stress conditions were comparable in each genotype (Figure 3a; Figure S11a). Indeed, the levels of typical drought stress-responsive metabolites, such as proline, raffinose, and *myo*-inositol, only slightly increased in wild type (Figure S12a). We could not observe marked effects on the metabolite profiles under our drought stress conditions. Nonetheless, the levels of several primary metabolites were altered in the RCAR lines under control and drought stress conditions (Figure S12b–d). A few of them showed similar changes in both RCAR lines. For instance, aspartic acid, succinate, and nicotinate levels were decreased in the RCAR6 and RCAR10 lines under control and drought conditions, whilst the glycerate level was increased. By contrast, several sugars, such as glucose, fructose, and trehalose, were more accumulated in the RCAR10 line.

Diurnal patterns of several primary metabolites were altered in the RCAR lines

Given that plant metabolites show strong diurnal variations (Annunziata et al., 2018; Gibon et al., 2006; Urbanczyk-Wochniak et al., 2005), we next analyzed whether we could observe any changes in the relative amounts (Figure 3) or the diurnal patterns. To examine whether the accumulation patterns were altered in the RCAR lines, *k*-means clustering was performed independently using the profiles of each genotype (Figure S13). The 38 annotated primary metabolites were classified into four groups, and most of them were classified into the same clusters regardless of the genotypes. For instance, Cluster 1 in wild type consisted of 14 metabolites harboring similar patterns during the five time points (Figure S13a). With the exception of sucrose and urea, these metabolites were clustered into the same group in the RCAR lines (Figure S13b,c). This result implied that the accumulation patterns of more than half of the annotated metabolites were not changed in the RCAR lines.

Taking into account the *k*-means clustering result, we first focused on the primary metabolites, whose levels were altered in the RCAR lines (Figure S14). Succinate, nicotinate, and glycerate levels were constitutively

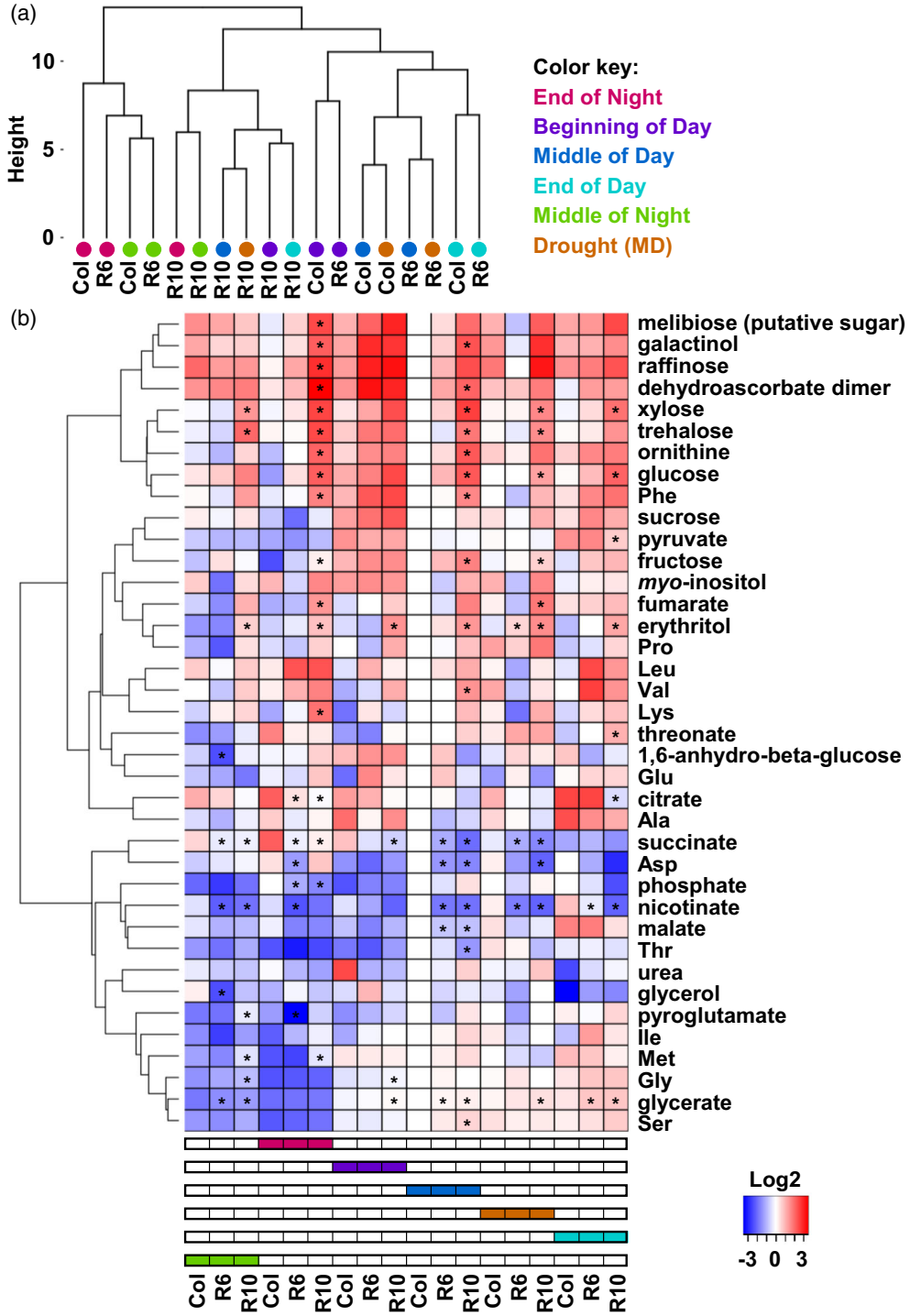

Figure 3. Primary metabolites differentially accumulated in the RCAR overexpressing lines.
Primary metabolites extracted from the leaf materials were analyzed by gas-chromatography mass-spectrometry. Chromatograms and mass spectra were evaluated using Chroma TOF 1.0 (LECO) and TagFinder 4.0 (Luedemann et al., 2008), and 38 metabolites were annotated. A putative sugar was annotated as melibiose.
(a) The metabolite profiles of Col-0, RCAR6-ox (R6) and RCAR10-ox (R10) lines were clustered by hierarchical cluster analysis using R.
(b) Heat map showing the relative accumulation of each metabolite compared to those in Col-0 harvested at the middle of the day (MD). For each metabolite, the value of Col-0 (MD) was set to 0. Asterisks shown on the columns of R6 and R10 lines indicate statistically significant differences ($P < 0.05$) compared to the corresponding Col-0 by single-factor ANOVA followed by a Tukey–Kramer *posthoc* test.

increased or decreased in both RCAR lines. In keeping with the previous report (Gibon et al., 2006), succinate and glycerate showed diurnal variations in wild type (Figure S14a). By contrast, the variations of succinate and glycerate levels were reduced or enhanced, respectively, in the RCAR lines. Although glycerate is one of the metabolites associated with photorespiration, glycine and serine levels, the glycine-serine ratio, and an index of photorespiration were unaltered in the RCAR lines (Figure S15). The levels of citrate, phosphate, aspartic acid, and malate also decreased in both RCAR lines at one time point (Figure S14b). The metabolic processes of these metabolites, including biosynthesis, catabolism, and transport, might be affected by the RCAR overexpression in a time-dependent manner.

In addition to these metabolites altered in both RCAR lines, several metabolites were more accumulated in the RCAR10 line (Figure S14c). Methionine was one of the amino acids showing diurnal variations (Gibon et al., 2006). The diurnal variation was observed in wild type and the RCAR6 line, but to a lesser extent in the RCAR10 line due to the higher level at night. Furthermore, six sugar and sugar alcohols, including glucose and trehalose, were constitutively accumulated in the RCAR10 line. The alterations observed in the RCAR10 line appeared to be gene-specific responses.

Next, we focused on the primary metabolites differently clustered in the RCAR lines (Figure S13) and examined the detailed accumulation patterns in each genotype (Figure S16). Although most of the metabolites did not show apparent variations, at least two showed slightly altered accumulation patterns in the RCAR lines. For instance, pyroglutamate accumulated in the light period in wild type, but the increase was faint in the RCAR lines. Although the amount was comparable among these genotypes at each time point, the accumulation of pyroglutamate in the light period might be impaired in the RCAR lines. Moreover, the decrease of threonate at dawn was not observed in the RCAR lines. These genotype differences suggest that besides the metabolites, whose levels were altered in the RCAR lines, the metabolic processes of pyroglutamate and threonate might be affected by the RCAR overexpression.

Integration of multi-omics profiles with PPI networks

Phosphoproteomic, proteomic, and metabolite profiles were changed by the RCAR overexpression (Figures 1–3). However, further integrative analyses were essential to investigate whether these changes were associated beyond biological hierarchies, i.e., protein phosphorylation and expression and primary metabolism, and determine the main target processes. Assuming that biologically relevant proteins physically interact with each other, we first derived the Arabidopsis PPI network from the STRING database, and the proteins differentially phosphorylated and expressed in the RCAR6 line were mapped on the network (Figures S17–S20). Given that fewer peptides were differentially phosphorylated under drought stress conditions (Figure 1), the PPI network was fragmental (Figure S17b). By contrast, more than 60 proteins, which were differentially phosphorylated under control conditions, were shown to be interacted in a large network (Figure S17a). Moreover, there were several submodules of functionally relevant proteins. In particular, the SRK2D, KIN10/11/12, and CIPK9 kinases formed the submodule via SNF4, a single hybrid βγ subunit of SnRK1 (Broeckx et al., 2016) (Figure 4a). The alterations of protein levels detected by the proteomic analysis were also integrated with the submodule, except for the kinase-interacting proteins, such as transcription factors, because none of them exhibited significant changes in protein levels (Figure 4b). As already described (Figure 2), the protein levels of

Figure 4. Integration of multi-omics profiles with protein–protein interaction networks and metabolic pathways.
(a) The protein–protein interaction (PPI) submodule of the kinases differentially phosphorylated in the RCAR6-ox (R6) line under control conditions. The entire network is shown in Figure S17(a). Colored filled circles represent differentially (false discovery rate [FDR] <0.01) phosphorylated peptides in the R6 line, and gray circles indicate those not changed or detected. A peptide was mapped to KIN10, KIN11 and KIN12, whilst these proteins were depicted by three separate circles according to the PPI data.
(b) A heat map showing the relative levels of proteins in the PPI submodule (a). The proteins detected by the proteomic analysis were listed, except for the kinase-interacting proteins, because none of them exhibited significant changes in protein levels. Each row represents a single peptide mapping to one or multiple proteins.
(c–e) Simplified schematic diagrams of photosynthetic metabolism (c), proline metabolism (d), and ammonia assimilation (e). Major changes in the phosphoproteomic, proteomic, and metabolite profiles at the middle of the day under control conditions were integrated. Colored arrows indicate the reactions in which the enzymes were differentially phosphorylated or expressed in the R6 line. The primary metabolites, which significantly increased or decreased in the R6 line, were indicated in red and blue, respectively. Dashed arrows represent conversions involving several steps.
(f, g) Heat maps showing the relative levels of differentially expressed proteins associated with carbon metabolism. The corresponding reaction number in the metabolic pathways are shown at the right end. Regardless of its actual functions, the plastidic NAD-dependent malate dehydrogenase (plNAD-MDH) was indicated for convenience. TRA2 and αCA1 were not shown in the pathways. The protein levels were shown in log2 fold-changes compared to those in Col-0 under control conditions. Asterisks denote statistically significant differences ($P<0.01$) compared to the Col-0 either under control or drought stress conditions by single-factor ANOVA using the Perseus. 2PGA, 2-phosphoglycerate; 3PGA, 3-phosphoglycerate; ADPG, ADP-glucose; DHAP, dihydroxyacetone phosphate; F6P, fructose-6-phosphate; FBP, fructose-1,6-bisphosphate; G1P, glucose-1-phosphate; G6P, glucose-6-phosphate; GABA, 4-aminobutyric acid; P5C, pyrroline-5-carboxylate; PEP, phospho*enol*pyruvate; RuBP, ribulose-1,5-bisphosphate; S7P, sedoheptulose-7-phosphate; SBP, sedoheptulose-1,7-bisphosphate; Suc6P, sucrose-6-phosphate; Tre6P, trehalose-6-phosphate; UDPG, UDP-glucose. Created with BioRender.com.

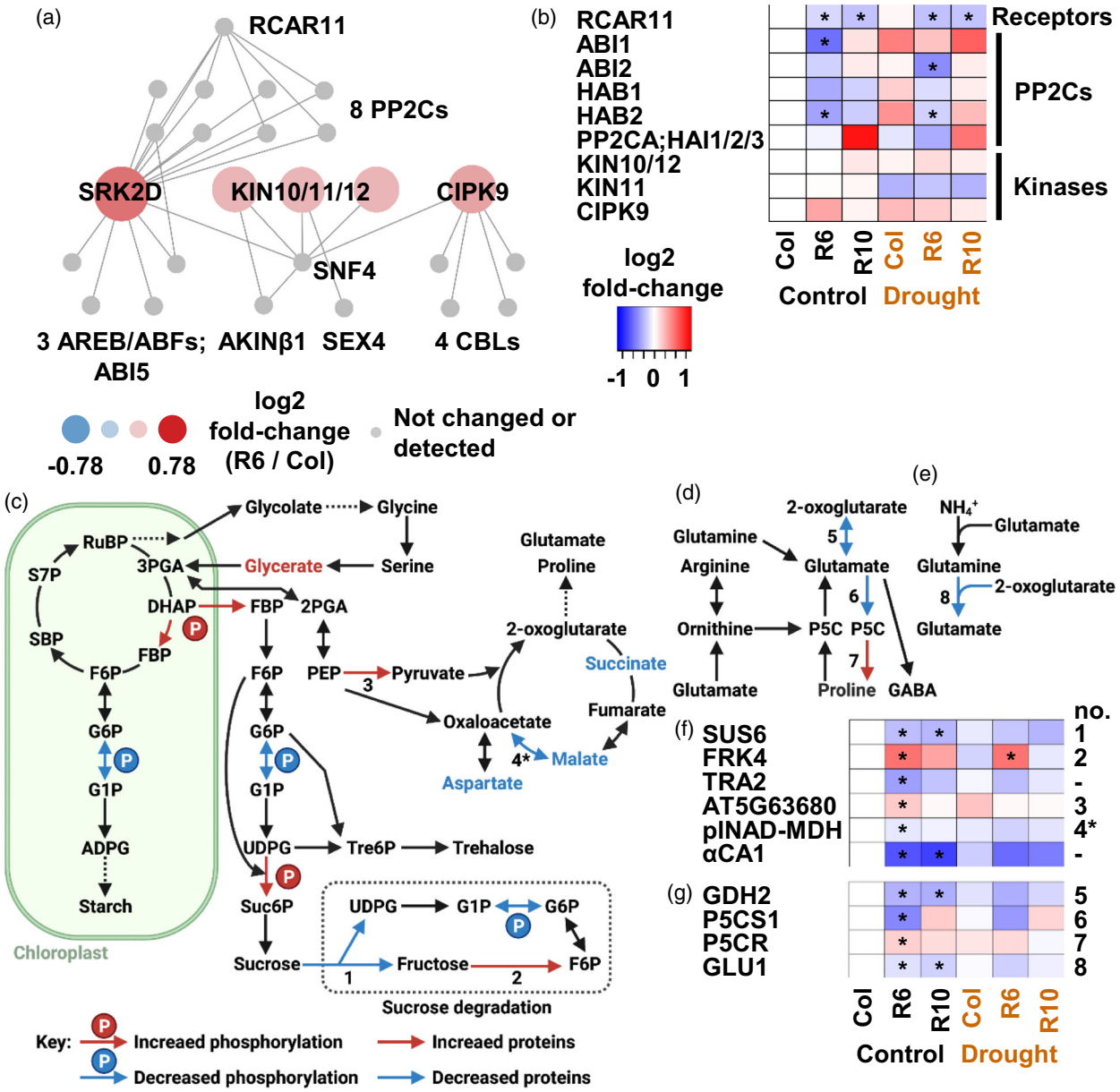

RCAR11, ABI1, ABI2, and HAB2 were significantly decreased in the RCAR6 line (Figure 4b). These data suggested that the RCAR6 overexpression decreased the PP2C protein levels constitutively, probably resulting in the increased phosphorylation of the SRK2D, KIN10/11/12, and CIPK9 kinases.

In the PPI submodules of the differentially phosphorylated proteins in the RCAR6 line (Figure S18), several proteins were also differentially expressed. Less than 20 proteins in the PPI network were differentially expressed (Figure S18d), implying that the phosphorylation affected by the RCAR6 overexpression might be involved in processes other than protein abundance regulation. By contrast, six exceptions, including FYVE4 in the vesicle trafficking submodule and AT3G49601 in the RNA processing submodule, were differentially phosphorylated and expressed in the RCAR6 line. The FYVE proteins harbor the zinc finger domain, named after Fab 1, YOTB, Vac1, and EEA1 proteins (Stenmark et al., 1996), interact with phosphatidylinositol 3-phosphate, and play important roles in endocytosis and vesicular trafficking (van Leeuwen et al., 2004). Interestingly, FYVE1 has recently been shown to be phosphorylated by the SnRK2 kinases and modulate ABA signaling at the perception and transcription (Belda-Palazon et al., 2016; Li et al., 2019). However, since FYVE1 and FYVE4 are distinct in the protein sequence

length and the FYVE domain position (van Leeuwen et al., 2004), further studies are required to reveal whether FYVE4 is regulated via phosphorylation and involved in ABA signaling. In addition to AT3G49601 encoding a possible pre-mRNA splicing factor, proteins associated with RNA processing, including SE and several SR proteins, were highly phosphorylated in the RCAR6 line (Figure S20b). Splicing regulators were suggested to be post-translationally regulated via phosphorylation and dephosphorylation (Reddy et al., 2013). Consistently, SE was shown to be a candidate substrate of SnRK2s (Yan et al., 2017). By contrast, SR45 was reported to be a splicing factor regulating glucose and ABA signaling (Carvalho et al., 2010) as well as the SnRK1 stability (Carvalho et al., 2016), although the SnRK1 proteins were unaltered by our proteomic analysis (Figure 4b). The splicing events up- and downstream of SnRK2 and SnRK1 kinases might be affected by the RCAR6 overexpression.

The differentially expressed proteins in the RCAR6 line were also mapped on the PPI network, and the submodules of ABA receptor complexes and vesicle trafficking were verified (Figures S19 and S20). Although the differentially phosphorylated proteins in the RCAR6 line were hardly found in these PPI networks, several submodules associated with histone acetylation, pyrimidine metabolism, proteolysis, and cellular respiration were observed. These processes might be affected via regulatory processes of protein abundance, such as mRNA processing.

Mapping of differentially phosphorylated and expressed proteins on metabolic pathways

The PPI networks of differentially phosphorylated and expressed proteins also determined the submodules associated with metabolic processes (Figures S17 and S19). The submodule of sulfur assimilation and glucosinolate (GSL) biosynthesis was verified, consistent with the GO analysis (Figure 2d; Figure S9). However, the proteins in these processes were not found to be differentially phosphorylated. By contrast, major changes associated with primary metabolism at the middle of the day under control conditions were integrated (Figure 4c–g). Enzymes of three reactions mediating sucrose synthesis from the Calvin-Benson cycle, including fructose-1,6-bisphosphate aldolases (FBAs), phosphoglucomutase 1 (PGM1), and sucrose-phosphate synthases (SPSs), were differentially phosphorylated, and two enzymes in sucrose degradation, sucrose synthase 6 (SUS6), and fructokinase 4 (FRK4), were differentially expressed. Although sugar contents were slightly but not significantly changed in the RCAR6 line, the rate of sugar metabolism might be affected via these enzymes. The carbon fixed in chloroplasts is also converted to organic acids and amino acids. The levels of aspartic acid and two intermediates of the tricarboxylic acid (TCA) cycle, succinate, and malate were decreased in the RCAR6 line, and a pyruvate kinase (AT5G63680) and a plastidic NAD-dependent malate dehydrogenase (pINAD-MDH) were differentially expressed. Yet, their enzymatic roles remain to be validated. The enzymes in proline metabolism and ammonia assimilation were also differentially expressed; however, the contents of the associated metabolites were unaltered (Figure 4d,e,g). Collectively, the integration of multi-omics profiles in the RCAR6 line suggested that parts of metabolic pathways, such as sucrose, organic acid, and amino acid metabolism, were altered via differentially expressed and phosphorylated enzymes.

DISCUSSION

Integrating multi-omics profiles is increasingly important to capture complex signaling networks controlled by various factors, including protein phosphorylation and abundance. We have previously shown that the overexpression of an ABA receptor, RCAR6, resulted in increased WUE without evident growth reductions (Yang et al., 2016). However, the underlying molecular mechanisms were largely obscure in this previous study. Here, we presented that phosphoproteomic, proteomic, and metabolite profiles in leaves were altered in the RCAR6 line. Moreover, our integrative analyses suggested that the decreased protein levels of PP2C coreceptors and the activation of the SnRK1 and SnRK2 kinases were the predominant processes caused by the RCAR6 overexpression, likely consistent with the model proposed by a recent study (Belda-Palazón et al., 2020). We analyzed the leaf materials under control and drought stress conditions (Figure S1), with the differences between the RCAR6 line and wild type being more prominent under control conditions (Figures 1–3). Clade A PP2C genes were responsive to ABA and drought stress (Fujita et al., 2009). Consistently, several PP2C proteins, including ABI1 and HAB2, were accumulated in wild type under drought stress conditions. By contrast, the phosphorylation of SRK2D, the ABA-activated kinase, was not significantly increased, and drought stress-responsive metabolites, such as proline, were not shown to be accumulated. These results implied that drought stress responses were moderately activated under the experimental conditions. ABA signaling was activated in the early stage under moderate drought stress conditions, while the ABA content decreased and the gene expression profile was adjusted in later stages (Harb et al., 2010). Therefore, the plants might be already acclimated after 9 days of water shortage, and the RCAR6 line appeared to respond to drought stress differently, as shown in the multi-omics profiles.

Sugar metabolism altered by RCAR6

Since identifying the core ABA signaling components, their roles beyond typical stress responses, such as stomatal

closure and stress-responsive gene expression, have been reported. For instance, the PP2C coreceptors were suggested to inhibit energy and ABA signaling in the absence of ABA via the direct interaction with the SnRK1 and SnRK2 kinases (Belda-Palazón et al., 2020; Rodrigues et al., 2013). A recent study further showed that the SnRK1 catalytic subunit was translocated from the nuclei to cytoplasm in response to ABA and inhibited the TOR activity (Belda-Palazón et al., 2022). While this model was proposed in roots and early seedlings, our results suggested that both SnRK1 and SnRK2 kinases were activated in leaves probably due to the decreased level of PP2Cs in the RCAR6 overexpressing line (Figure 4), confirming and extending the model. Yet, since the phosphorylation of SRK2D, but not that of KIN10/11/12, was significantly increased in the RCAR10 line under control conditions, albeit biological replicates were insufficient for the RCAR10 line (Figure 1), whether the model (Belda-Palazón et al., 2020) works under all Arabidopsis 14 RCARs remains obscure. SPSs were one of the characterized substrates of SnRK1 (Nukarinen et al., 2016), and the same serine residues of SPS1F and SPS4F were highly phosphorylated (Figure S3). Given that spinach SPS was inactivated by phosphorylation (Sugden et al., 1999), the sucrose 6-phophate synthesis might be inhibited. Moreover, the phosphorylated threonine of FBAs increased as well as the SnRK2 activation (Figure S3), likely consistent with the decreased phosphorylation of FBA8 in the triple *snrk2* mutant (Umezawa et al., 2013), albeit the phosphosites were different. Although little is known about whether their substrates are distinct or overlapping, the SnRK1 and SnRK2 kinases appeared to be involved in the regulation of sucrose synthesis from the Calvin-Benson cycle. The enzymes in sucrose degradation, SUS6 and FRK4, were also differentially expressed; however, sugar contents were only slightly altered in the RCAR6 line (Figure 3). SnRK1 activity is inhibited by sugar phosphates, such as glucose 6-phosphate and trehalose 6-phosphate (Nunes et al., 2013; Toroser et al., 2000; Zhang et al., 2009). Therefore, further studies, such as the absolute quantification of phosphorylated intermediates by LC–MS/MS, will be essential to obtain a deeper understanding of how sugar metabolism is affected in response to ABA.

Several sugar transporters were also differentially phosphorylated or expressed. Two vacuolar monosaccharide transporters, TONOPLAST MONOSACCHARIDE TRANSPORTER 1 (TMT1; AT1G20840) and AT1G19450, were differentially phosphorylated, and the TMT1 protein also decreased in the RCAR6 line (Tables S1 and S6). A structural characteristic of TMT transporters is a large centrally located hydrophilic loop, in which several phosphorylation sites were reported in Arabidopsis and barley (Endler et al., 2009; Schulze et al., 2012; Whiteman et al., 2008). TMT1 was involved in sugar partitioning into the vacuole, and its activity was associated with growth and seed yield (Wingenter et al., 2010) and suggested to be activated via phosphorylation of the loop (Wingenter et al., 2011). TMT1 showed decreased phosphorylation in the loop (Ser319) and protein abundance, implying that sugar partitioning into the vacuole was constrained. Given that the SnRK1 kinases are the sensors in response to energy deficit and starvation, TMT1 might be inhibited to provide consumable sugars for maintaining metabolism running, yet whether SnRK1s regulate TMT1 remains unclear.

Contrary to SnRK1, the TARGET OF RAPAMYCIN (TOR) kinase is activated in response to nutrient availability and promotes cell proliferation and growth (Xiong & Sheen, 2014). Although SnRK1 and SnRK2 were reported to inhibit TOR signaling via direct phosphorylation (Belda-Palazón et al., 2022; Nukarinen et al., 2016; Wang et al., 2018), representative TOR signaling components (Xiong & Sheen, 2014) were not found to be differentially phosphorylated or expressed in our large-scale profiles (Tables S1 and S6). Alterations of some substrates of SnRK1 and SnRK2 might not be detected because of low protein abundance and rapid reversible phosphorylation and dephosphorylation. Nonetheless, ones of the targets of TOR signaling (Caldana et al., 2013; Moreau et al., 2012; Ren et al., 2012), expansins decreased in the RCAR6 line, albeit fewer expansin proteins decreased in the RCAR10 line (Figure S8). The SnRK1 kinase was also an upstream regulator inhibiting the expansin gene expression (Baena-González et al., 2007). By contrast, an earlier study suggested that the expansin gene expression induced at low water potentials was not ABA dependent (Wu et al., 2001), whilst ABA was reported to induce the expansin activity via transcriptional regulation (Zhao et al., 2012), possibly consistent with the presence of ABA-responsive *cis*-elements in their promoters (Valenzuela-Riffo et al., 2020). Therefore, whether ABA works as an upstream signal of expansins remains debatable. However, several α expansin genes, *EXPA*s, have been reported to serve as good indices of leaf growth being induced and repressed under moderate and severe drought stress conditions, respectively (Clauw et al., 2015; Harb et al., 2010). Given that the rosette size and the leaf expansion rate in the RCAR6 and RCAR10 lines were comparable with wild type (Yang et al., 2016), the differentially phosphorylated and expressed proteins, including expansins and others in sugar metabolism and transport, respiration, and mitosis (Figures S17 and S19) might be favorable targets to address whether, and if so how, cell growth is affected in ABA signaling.

Stomatal regulation downstream of RCAR receptors

Stomata are responsible for transpiration and gas exchanges, and thus one of the determinants of plant WUE, as observed in the RCAR6 and RCAR10 lines showing a stomatal closing phenotype (Yang et al., 2016). The

stomatal aperture is controlled by various environmental and endogenous cues, including ABA, blue light, and carbon metabolism, and our multi-omics profiles provided insights into the molecular mechanisms downstream of RCARs. Given that subclass III SnRK2s, including SRK2D, are the pivotal activators of ABA signaling (Fujii & Zhu, 2009; Fujita et al., 2009), the activated SRK2D (Figure 1) might play the predominant role in stomatal closure, although their substrates, such as SLOW ANION CHANNEL-ASSOCIATED 1 (SLAC1), were not found to be differentially phosphorylated. The SnRK2s were also involved in water transport in guard cells via the phosphorylation of an aquaporin, PLASMA MEMBRANE INTRINSIC PROTEIN 2;1 (PIP2;1) (Grondin et al., 2015). Therefore, it was worth noting that two PIP2s, PIP2;3 (AT2G37180) and PIP2;6 (AT2G39010), were differentially phosphorylated or expressed in the RCAR6 line (Tables S1 and S6). While the decrease of the PIP2;3 protein was not observed in the RCAR10 line, the N-terminus Thr7 and Ser13 of PIP2;6 was found to be highly phosphorylated in both RCAR6 and RCAR10 lines. Our results postulated that RCAR6 and RCAR10 were involved in water management in guard cells through these membrane proteins.

As a phytohormone which stimulates stomatal closure, the inhibitory roles of ABA in the stomatal opening have also been studied, especially in interaction with blue light signaling (Inoue & Kinoshita, 2017). A mechanistic explanation for how blue light and ABA function antagonistically was provided by a recent study demonstrating that the phosphorylation of plasma membrane H^+-ATPases was required for both light-promoted stomatal opening and ABA-induced stomatal closure (Pei et al., 2022). Blue light stimulates stomatal opening via the blue-light receptor kinases, phototropins, which are activated by autophosphorylation in response to blue light. Notably, the conserved serine of PHOT1 and PHOT2 were highly phosphorylated in the RCAR6 and RCAR10 lines (Figure S4). These sites were not found in the pioneering studies exploring the phosphorylation sites of PHOT1 (Inoue et al., 2008; Sullivan et al., 2008). However, the following research showed that the Ser450 of PHOT1 was phosphorylated in response to blue light (Deng et al., 2014). Moreover, the corresponding Ser376 of maize ZmPHOT1 was shown to be phosphorylated and involved in phototropism (Suzuki et al., 2019). Together with a report that PHOT1 and PHOT2 were decreased in transcript or protein levels in response to ABA, presumably depending on light conditions (Eckstein et al., 2016), our phosphoproteomic data implied that phototropins were regulated in ABA signaling in multiple ways. Blue light responses, including stomatal opening, might be altered in the RCAR6 and RCAR10 lines due to the increased phosphorylation of phototropins, although further studies are necessary.

In addition to the signaling network regulated by ABA and blue light, the stomatal aperture is actively controlled through carbon metabolism in guard cells as well as mesophyll cells (Daloso et al., 2017). The increased atmospheric CO_2 stimulates stomatal closing via bicarbonate produced by β carbonic anhydrases (CAs) (Hu et al., 2010). Although αCA1 decreased in RCAR lines (Figure 4), its role remains uncertain because αCAs have been scarcely characterized in plants. Organic acid metabolism also plays a role in stomatal regulation, and malate is one of the counter-ions of K^+ accumulating in the vacuole of guard cells during stomatal opening. In the metabolite profiles of RCAR lines, one of the most pronounced changes was a constitutive decrease of succinate (Figure 3). Moreover, other intermediates of the TCA cycle, such as citrate and malate, were also differentially accumulated in both RCAR lines (Figure S14). The role of succinate in stomatal regulation has yet to be demonstrated; however, the study of maize hybrids grown under greenhouse conditions reported that the succinate level was negatively and positively correlated with leaf temperature and stomatal conductance, respectively, after withholding water (Witt et al., 2012). The increased succinate content was also observed in the transgenic tomato, in which the iron–sulfur subunit of succinate dehydrogenase in the TCA cycle was manipulated, which exhibited an enhanced CO_2 assimilation via elevated stomatal conductance and aperture (Araújo et al., 2011). Among the primary metabolites showing a diurnal accumulation pattern, malate and fumarate increase during the day, and succinate decreases (Gibon et al., 2006). Therefore, our results raised the hypothesis that the succinate pool at dawn was consumed via the TCA cycle to produce enough malate for an adequate stomatal opening during the day. Conversely, the shortage of succinate at dawn, as in RCAR lines (Figure S14a), might constrain the malate production, resulting in improper stomatal opening. Previously, we suggested that that the cytosolic *FUMARASE 2* (*FUM2*) was transcriptionally regulated downstream of the SnRK2s (Yoshida, Obata, et al., 2019). Our present proteomic profile also suggested that a pyruvate kinase (AT5G63680) and plNAD-MDH were possible targets downstream of RCAR6, albeit these proteomic changes were vague in the RCAR10 line (Figure 4). In particular, plNAD-MDH was proposed to play an important role in the malate valve during darkness, a crucial mechanism for balancing metabolic fluxes by enabling the indirect transfer of reducing equivalents among subcellular organelles (Selinski & Scheibe, 2019). Although future characterization of the role of these enzymes in ABA signaling is necessary, our results indicate that ABA might be involved in the stomatal closing through various targets, including aquaporins, phototropins, and organic acid metabolism.

Post-translational protein modifications downstream of RCAR6

Technical advances in concentrating, detecting, and quantifying phosphopeptides enable us to profile a global change of protein phosphorylation, which is a crucial post-translational modification in cell signaling. Protein phosphorylation is proceeded by kinases, and their activities are also regulated via phosphorylation. The phosphoproteomic profile of the RCAR6 line revealed that a large number of kinases were differentially phosphorylated (Figure 1; Table S2), suggesting that their signaling pathways were affected as well. Importantly, the increased phosphorylation of the SnRK2 and SnRK1 kinases and the altered phosphorylation of their substrates suggested that these signaling pathways were activated in the RCAR6 line, albeit these changes were less evident in the RCAR10 line. By contrast, the SP motif was enriched in the phosphopeptides altered in the RCAR6 line, and this motif was one of the enriched motifs downstream of the SnRK2 and SnRK1 kinases (Nukarinen et al., 2016; Umezawa et al., 2013; Wang et al., 2013). Although the meta-analysis of Arabidopsis phosphoproteome data suggested that the SP motif was a common target for several kinases (van Wijk et al., 2014), the motif was well-documented as the major phosphorylation site for proline-directed kinases, including MAP kinases, verified by a phosphoproteomic study exploring MAP kinase substrates in Arabidopsis (Hoehenwarter et al., 2013). Given that several upstream kinases in the MAP kinase cascade, such as MAPKKKs, were differentially phosphorylated in the RCAR6 line (Table S2), it was postulated that the MAP kinase signaling was also affected by the RCAR6 overexpression. Indeed, several MAPKKKs were reported to be confirmed or possible substrates of the SnRK2s in ABA signaling (Kamiyama et al., 2021; Tajdel et al., 2016). Moreover, the SnRK1 kinase was involved in the regulation of MAPK6 (also known as MPK6) via direct interaction (Cho et al., 2016), and a MAPKKK was identified in the SnRK1 PPI network (Carianopol et al., 2020). The kinases in the MAP kinase cascade identified in the present study may be attractive targets to address an undetermined mechanism of how the signaling pathways of SnRK2, SnRK1 and MAP kinases are connected to each other.

In addition to the activation of the SnRK1 and SnRK2 signaling pathways, CIPK9 appeared to be activated via the increased phosphorylation of the conserved threonine (Figure S4). CIPKs are the kinases interacting with the CBL calcium sensors, and CIPK9 was shown to be involved in low K^+ responses (Pandey et al., 2007). Contrary to other CIPKs, such as CIPK23, which are regulated by clade A PP2Cs (Lee et al., 2007; Léran et al., 2015), CIPK9 was suggested to be specifically regulated by a clade B PP2C, namely AP2C1 (Singh et al., 2018). Therefore, unlike SnRK1s and SnRK2s, the decreased clade A PP2Cs might not activate CIPK9. However, CIPK9 was reported to be directly or indirectly associated with SnRK2s and RCARs in ABA signaling. Indeed, a study exploring the interacting proteins of SnRK2s revealed that SRK2D interacted with CIPK9 and other CIPKs (Mogami et al., 2015). Moreover, RCAR11, which decreased in the RCAR lines (Figure S7), interacted with AP2C1 (Jones et al., 2014). Further studies on CIPK9 may shed light on how ABA and calcium signaling are interconnected.

Ubiquitylation is another conserved and reversible post-translational modification involved in many cellular processes, including proteolysis and regulation of protein interactions and localizations (Komander & Rape, 2012). Several proteins mediating ubiquitylation were reported to regulate the core components of ABA signaling (Yoshida, Christmann, et al., 2019), indicating that its signal transduction is fine-tuned via ubiquitylation. Our proteomic profile revealed that proteins in proteolysis, including UBIQUITIN-SPECIFIC PROTEASE 7 (UBP7), were differentially expressed in the RCAR6 line (Figures S19 and S20). UBPs are a family of deubiquitylation enzymes, and one of 27 Arabidopsis UBPs (Liu et al., 2008), UBP24, was also differentially phosphorylated (Table S1). Whilst UBP24 was involved in the regulation of the phosphatase activity of PP2Cs via its uncharacterized substrates (Zhao, Zhou, et al., 2016), UBP7 and its homolog UBP6 were shown to regulate the stability of the plant immune coactivator NONEXPRESSOR OF PATHOGENESIS-RELATED (PR) GENES 1 (NPR1) (Skelly et al., 2019). Although NPR1 was not found in the differentially expressed proteins (Table S6), proteolytic processes might be manipulated via these ubiquitylation-associated proteins in ABA signaling downstream of RCAR6. It was also noteworthy that ubiquitylated RCARs were targeted to endosomal trafficking through FYVE1 (Belda-Palazon et al., 2016; Bueso et al., 2014). Yet, the role and substrates of FYVE4, which was differentially phosphorylated and expressed by the RCAR6 overexpression (Figure S18), have not been elucidated in ABA signaling. However, future studies on proteolysis and ubiquitylation will be required to address the open question of why the protein levels of PP2Cs, especially ABI1 and ABI2, decreased in the RCAR6 line but not the RCAR10 line (Figures 2c and 4b), and thereby reveal how the ABA receptor complexes are turned over.

We mainly discussed above the shared characteristics in phosphoproteomic, proteomic, and metabolite profiles in RCAR6 and RCAR10 lines in order to explore key factors associated with their phenotypes of an increased WUE with high growth rates. By contrast, there were differences between these RCAR lines. Although PCA covers parts of data after dimensionality reduction, the plots implied that the alterations in the RCAR lines were somewhat complex, not simply explained by their overexpression levels. For

instance, the proteomic profiles of RCAR6 and RCAR10 lines under control conditions appeared to be plotted at opposite sides compared to wild type (Figure S7b). A similar plotted pattern was also observed in the metabolite profiles at the middle of night (Figure S11a). Although subclass II RCARs, including RCAR6 and RCAR10, exhibited comparable growth phenotypes related to WUE (Yang et al., 2016), overlapping but distinct molecular processes might be stimulated by their overexpression. Careful validations will be necessary to examine whether the differences in phosphoproteomic, proteomic, and metabolite profiles between RCAR6 and RCAR10 lines were derived from their receptor characteristics, such as their affinities with ABA and coreceptors, or their overexpression levels.

Concluding remarks

Abscisic acid is one of the phytohormones that stimulate obvious changes in gene expression, and thus, a large amount of transcriptome data is publicly available. Typical ABA-induced genes include those encoding functional proteins, such as late embryogenesis abundant proteins and enzymes in osmoprotectant synthesis, and signaling proteins, such as transcription factors, kinases and phosphatases (Fujita et al., 2011). By contrast, albeit profiles of low abundant proteins, such as transcription factors, were unknown because of current technical limitations, our GO and integrative analyses implied that different groups of proteins, such as those in mRNA splicing and secondary metabolism, were differentially phosphorylated or expressed by the RCAR overexpression. Although further validations are required, these alterations might not necessarily require transcriptional regulation. Therefore, our datasets appeared to be essential pieces of information to unveil comprehensive molecular events, including transcriptions and post-translational modifications, in ABA signaling. Future studies combined with transcriptome analyses will uncover which changes in transcript, protein, phosphorylation, and metabolite levels or any combinations of them are crucial for the water-productive growth of the RCAR lines.

Sugar and ABA signaling have long been thought to be linked, as evidenced by the glucose-insensitive phenotypes of the mutants of the ABA biosynthesis and signaling genes (Arenas-Huertero et al., 2000; Laby et al., 2000; Rook et al., 2001). Yet, it remains debatable how these signaling pathways are associated. Based on the altered phosphoproteomic, proteomic and metabolite profiles in the RCAR6 overexpressing Arabidopsis, we demonstrated that the SnRK1 and SnRK2 kinases in energy and stress signaling pathways, respectively, were under the control of ABA receptor-coreceptor complexes, confirming and extending the recently proposed model (Belda-Palazón et al., 2020, 2022). Moreover, we demonstrated that candidate enzymes and metabolites downstream of SnRK1 and SnRK2. The proteins of the PP2C coreceptors might decrease constitutively in the RCAR6 line, and thus the SnRK1 and SnRK2 appeared to be kept active. Although the substrates and downstream pathways of SnRK1 and SnRK2 have hardly been compared because of their independent studies so far. It will be important to address their spatial and temporal activation patterns in order to redefine their roles in sugar and ABA signaling. Our data further propose that energy- and water-saving mechanisms might be activated simultaneously in response to water shortage due to the same inhibitory module of ABA receptors and coreceptors. It will be important to validate this for developing crops that are efficient in energy and water usage.

EXPERIMENTAL PROCEDURES

Plant material and growth conditions

Arabidopsis (*A. thaliana*) Col-0 ecotype was used as the wild type. The RCAR6 and RCAR10 overexpressing Arabidopsis were generated previously (Yang et al., 2016). Plants were grown under the conditions, under which relative soil water contents (SWCs) (v/v) were determined gravimetrically, as described before (Yang et al., 2016, 2019). In brief, seeds were germinated on half-strength Murashige and Skoog (0.5 MS) agar plates, and seedlings were grown for 7 days under the continuous-light conditions of 60 $\mu mol\, m^{-2}\, sec^{-1}$ photon flux density. Individual seedlings were transferred to 200-ml plastic pots filled with 33.4 g dry soil (Classic Profi Substrat, Einheitserde Werkverband, Germany) supplemented with 140 g water, which corresponded to a SWC of 70% v/v, i.e. $\Psi > -0.07$ MPa. Plants were grown in a growth cabinet (Conviron E15, Winnipeg, Canada) under short-day conditions (8-h light and 16-h dark) of 150 $\mu mol\, m^{-2}\, sec^{-1}$ photon flux density at 22°C and 50% relative humidity (RH) during the day and 17°C and 60% RH at night. Six-week-old plants were grown for nine more days under the same watering conditions under which water was administrated repeatedly to keep SWC ≥70% ($\Psi > -0.07$ MPa). Moderate water scarcity treatments without leaf wilting, which were defined as drought stress in this study, were achieved by growing plants under well-watered conditions followed by discontinuation of watering for 9 days (SWC $27.9 \pm 1.7\%$, $-0.13 < \Psi < -0.1$ MPa) (Figure S1). Leaf materials were harvested at the end of the night (EN), the beginning of the day (BD), the middle of the day (MD), the end of the day (ED), and the middle of the night (MN). The leaf materials of plants treated with drought stress were also harvested at MD. Two to four biological replicates for protein samples were harvested at MD under control and drought stress conditions. Five to seven replicates for metabolite samples were harvested at five time points under control conditions and at MD under drought stress conditions (Figure S1b). Each harvesting was immediately frozen in liquid nitrogen and stored at −80°C until further processing.

Protein lysis and digest

Protein lysis and digest were performed as described (Mergner et al., 2020) with minor modifications. In brief, proteins from homogenized leaf materials were precipitated overnight with 10% trichloroacetic acid in acetone at −20°C and subsequently washed three times with ice-cold acetone. Dry samples were incubated with urea digestion buffer (8 M urea, 50 mM Tris–HCl pH 8.5, 1 mM

DTT, cOmplete™ EDTA-free protease inhibitor cocktail [Roche, Basel, Switzerland], in-house phosphatase inhibitor) for 1 h. Protein concentration was determined with a Bradford assay (1976). For each sample, 210 μg of protein input was used. For the shared normalization channel of the control and drought TMT batches, 24 μg from each sample were mixed. Samples were reduced (10 mM DTT), alkylated (55 mM chloroacetamide), and diluted 1:7 with digestion buffer (50 mM Tris–HCl pH 8.5, 1 mM $CaCl_2$). In-solution digestion with trypsin (1:100 w/w) (Roche) was performed at 37°C for 4 h followed by a second digestion step overnight. Digested samples were acidified with trifluoroacetic acid (TFA) and centrifuged at 14 000 ***g*** for 15 min at 4°C. The supernatants were desalted on 50 mg SepPAC columns (Waters, Milford, USA) and vacuum-dried. TMT10plex labeling (Lot. SK260195) was performed as described (Ruprecht, Zecha, et al., 2017; Zecha et al., 2019). The respective sample volume for the Control (TMT10plex channels, Col-0: 126, 127N, 127C; RCAR6: 128C, 129N, 129C, 130N, RCAR10: 128N, 130C, mix: 131) and Drought (TMT10plex channels, Col-0: 126, 127N, 127C; RCAR6: 128N, 128C, 129N, RCAR10: 129C, 130N, 130C, mix: 131) experiments were combined according to a preliminary mixing test analysis. The combined TMT samples were desalted and vacuum-dried prior to phosphopeptide enrichment.

Peptide enrichment and off-line fractionation

Fe^{3+}-ion metal affinity chromatography (IMAC) was performed as described (Ruprecht, Koch, et al., 2017) with minor adjustments. TMT-labeled peptides were re-suspended in IMAC loading buffer (0.1% TFA, 30% acetonitrile). The enrichment was performed with wash Buffer A (0.07% TFA, 30% acetonitrile) and elution Buffer B (0.315% NH_4OH). Collected full proteome and phosphopeptide fractions were vacuum-dried and stored at −80°C until further use.

Phosphopeptides were fractionated into four fractions using the high pH reversed-phase protocol and pooling scheme for TMT-labeled phosphopeptides as described (Ruprecht, Zecha, et al., 2017). Phosphopeptide fractions were reconstituted in 0.1% FA and loaded on self-packed StageTips (five disks, Ø 1.5 mm C18 material, 3 M Empore™). After a wash step with 0.1% FA, basic reversed phase buffer A (25 mM NH_4FA pH 10) was applied to the StageTips, and the flow-through was collected in a new vial. Phosphopeptides were eluted with 5%, 10%, 15%, 17.5%, and 50% acetonitrile in 25 mM NH_4FA pH 10. The 5% and 50% acetonitrile and the flow through and 17.5% fractions were combined, and all fractions were dried down prior to LC–MS/MS analysis.

For the full proteome analysis, the IMAC flow-through fraction was reconstituted in 10 mM ammonium acetate, pH 4.7, and an equivalent of 100 μg protein digest separated with trimodal mixed mode chromatography on an Acclaim Trinity P1 2.1 × 150 mm, 3-μm column (Thermo Fisher Scientific, Waltham, USA) using a Dionex Ultimate 3000 HPLC system (Dionex Cor., Idstein, Germany). A total of 32 fractions were collected, vacuum-dried, and stored at −20°C until LC–MS/MS analysis.

LC–MS/MS analysis and data processing

Nanoflow LC–MS/MS was performed using a Dionex 3000 (Thermo Fisher Scientific) system coupled to a QExactive Orbitrap HF-X (Thermo Fisher Scientific). Peptides were reconstituted in 0.1% FA (full proteome) or 0.1% FA, 50 mM citrate (phosphoproteome), respectively, delivered to a trap column (75 μm i.d. × 2 cm, packed in-house with 5 μm of Reprosil C18 resin; Dr. Maisch, Germany) and washed using 0.1% formic acid at a flow rate of 5 μl min^{-1} for 10 min. Subsequently, peptides were transferred to an analytical column (75 μm i.d. × 45 cm, packed in-house with 3 μm Reprosil C18 resin; Dr. Maisch, Germany) at a flow rate of 300 nl min^{-1}. Peptides were chromatographically separated using a linear gradient of solvent B (0.1% formic acid, 5% DMSO in ACN) and solvent A (0.1% formic acid, 5% DMSO in water) from 4 to 32% of B in 50 min. The total measurement time for each sample was 60 min.

The instrument was operated in data-dependent mode, automatically switching between MS and MS2 scans. Full scan MS spectra (m/z 360–1300) were acquired with a maximum injection time of 10 msec at 60 000 resolution and an automatic gain control (AGC) target value of 3e6 charges. For the top 25 precursor ions, high-resolution MS2 spectra were generated in the Orbitrap with a maximum injection time of 55 msec at 45 000 resolution (isolation window 0.8 m/z), an AGC target value of 2e5 and normalized collision energy of 33%. The intensity threshold was set to 1.8e4 with a dynamic exclusion of 25 sec. Only precursors with charge states between 2 and 6 were selected for fragmentation.

Raw data files for full proteome and phosphoproteome analyses were processed together as two separate parameter groups using MaxQuant software (version 1.5.8.3) with MS2-based quantification settings unless otherwise described (Tyanova, Temu, & Cox, 2016). Parent Ion Fraction (PIF) was set to 0.75 and TMT batch correction factors as specified by the manufacturer (Lot. SK260195). MS/MS spectra were searched against Araport11 protein-coding genes (Araport11_genes.201606.pep.fasta; download 06/2016) (Cheng et al., 2017) and known contaminants, with trypsin as protease and up to two allowed missed cleavages. Carbamidomethylation of cysteines was set as a fixed modification, and oxidation of methionines and N-terminal acetylation as variable modifications. For the phosphoproteome parameter group, phosphorylation of serine, threonine, or tyrosine was also added as a variable modification. Results were filtered to 1% peptide-spectrum match, site and protein FDR. The raw mass spectrometry data and MaxQuant result files have been deposited to the ProteomeXchange Consortium via PRIDE (Vizcaíno et al., 2016), with the dataset identifier PXD042054 (Reviewer login: reviewer_pxd042054@ebi.ac.uk, password: TqSN4hWn).

Data analysis

Protein abundance estimation was based on corrected TMT reporter intensities and total sum normalized for each full proteome sample. The phosphorylation site intensities were normalized with the full proteome total sum intensity ratios. Unless otherwise stated, displayed protein and phosphorylation site abundances were log2 transformed. Results from the two TMT batches were aligned using row-wise normalization with correction factors calculated from the shared mix channel. The mix channels (TMT-131) were subsequently removed for all further analyses of the TMT datasets. Basic statistical analyses were performed on the Perseus platform (version 1.5.5.3; 2.0.5.0) (Tyanova, Temu, Sinitcyn, et al., 2016). ANOVA analysis of differentially abundant phosphorylation sites and proteins among genotypes within the control and drought TMT dataset was performed using total-sum normalized log2 transformed reporter intensities and the Multiple-sample test function in Perseus (s0 = 0, $P < 0.05$; all other settings were left as default) (Data S1). Subsequently, a post hoc Tukey's HSD test for one-way ANOVA was performed with Perseus 2.0.5.0 to identify significant differences (FDR <0.01) among the RCAR6 and RCAR10 lines and Col-0. GO analyses were performed using the ShinyGO (version 0.77; http://bioinformatics.sdstate.edu/go/) (Ge et al., 2020) with preset parameters (FDR cutoff <0.05), except minimal Pathway size was set to 10. Motifs representing amino acid preferences flanking the phosphorylation sites were discovered using the MoMo web server (https://meme-suite.org/meme/tools/momo)

(Cheng et al., 2019). The motif-x algorithm (Schwartz & Gygi, 2005) was employed with preset parameters, and the motifs (adjusted *P*-value <0.01) were considered to be significantly enriched.

Analysis of primary metabolites using GC–MS

Aliquot leaf samples (≈100 mg) were homogenized using a ball mill precooled with liquid nitrogen and extracted in 1400 µl of methanol. Subsequently, 60 µl of internal standard (0.2 mg ribitol ml^{-1} water) was added as a quantification standard. The extraction, derivatization, standard addition, and sample injection were conducted as described (Lisec et al., 2006) with minor modifications in the equipment. An autosampler Gerstel Multi-Purpose system (Gerstel GmbH & Co., KG, Germany) was used to inject the samples to a chromatograph coupled to a time-of-flight mass spectrometer system, Leco Pegasus HT TOF-MS (LECO Corporation, St. Joseph, MI, USA). Metabolites were identified by comparison to database entries of authentic standards (Kopka et al., 2005). Chromatograms and mass spectra were evaluated using Chroma TOF 1.0 (LECO) and TagFinder 4.0 software (Luedemann et al., 2008). The relative content of metabolites was calculated by normalization of signal intensity to that of ribitol, which was added as an internal standard, and by the dry weight of the material, which was independently measured. All data were also processed using the Xcalibur 4.0 software (Thermo Fisher Scientific) to verify the metabolite identification and annotation. Data presentation and experimental details are provided in Data S2 following current reporting standards (Fernie et al., 2011). For *k*-means clustering, number of clusters, k ($\approx\sqrt{N/2} = 4.36$), was determined according to the crude rule of thumb (Mardia et al., 1979).

PPI mapping

The *A. thaliana* PPI network (v11.5) was derived from the STRING database (https://string-db.org/) (Szklarczyk et al., 2019), and the interactions (confidence score >0.95) were studied. Networks were drawn using the Cytoscape software (Shannon et al., 2003).

ACCESSION NUMBERS

The Arabidopsis Genome Initiative locus numbers for the major genes discussed in this article are as follows: ABI1 (AT4G26080), ABI2 (AT5G57050), CIPK9/SnRK3.12 (AT1G01140), FBA2 (AT4G38970), FBA4 (AT5G03690), FBA5 (AT4G26530), FBA6 (AT2G36460), FBA8 (AT3G52930), FRK4 (AT3G59480), HAB2 (AT1G17550), KIN10/SnRK1.1 (AT3G01090), KIN11/SnRK1.2 (AT3G29160), KIN12/SnRK1.3 (AT5G39440), PGM1 (AT5G51820), PHOT1 (AT3G45780), PHOT2 (AT5G58140), pINAD-MDH (AT3G47520), RCAR10/PYL4 (AT2G38310), RCAR11/PYR1 (AT4G17870), RCAR6/PYL12 (AT5G45870), SPS1F (AT5G20280), SPS4F (AT4G10120), SRK2D/-SnRK2.2 (AT3G50500), SUS6 (AT1G73370), αCA1 (AT3G52720).

AUTHOR CONTRIBUTIONS

TY and EG designed the research and wrote the article; TY performed the data analysis and integration; JM performed LC–MS/MS experiments under the supervision of BK; TY and ARF performed GC–MS analysis; ZY and JL prepared plant materials; all authors read and approved the article.

ACKNOWLEDGEMENTS

We thank Saleh Alseekh for his assistance with GC–MS. This work was supported by Deutsche Forschungsgemeinschaft (DFG) (No. 460915364 to T.Y.), the Max-Planck Society (to A.R.F.) and SFB924 (to B.K. and E.G.). Open Access funding enabled and organized by Projekt DEAL.

CONFLICT OF INTEREST

No conflict of interest declared.

SUPPORTING INFORMATION

Additional Supporting Information may be found in the online version of this article.

Data S1. (a) CONTROL_Phosphorylation sites and ANOVA test (s0 = 0, *P*-value <0.05). (b) DROUGHT_Phosphorylation sites and ANOVA test (s0 = 0, *P*-value <0.05). (c) Shared_Phosphorylation sites CONTROL and DROUGHT dataset. (d) CONTROL_Proteins and ANOVA test (s0 = 0, *P*-Value <0.05). (e) DROUGHT_Proteins and ANOVA test (s0 = 0, *P*-value <0.05). (f) Shared_Proteins CONTROL and DROUGHT dataset.

Data S2. Metabolite data report for the compounds analyzed in this study.

Figure S1. The experimental design for multi-omics profiling.

Figure S2. Phosphoproteomic profiles are altered in the RCAR overexpressing lines.

Figure S3. The substrates of SnRK2 and SnRK1 kinases are differentially phosphorylated in the RCAR overexpressing lines.

Figure S4. A calcineurin B-like-interacting protein kinase and phototropins are differentially phosphorylated in the RCAR overexpressing lines.

Figure S5. The phosphosites differentially phosphorylated under drought stress conditions.

Figure S6. Drought-stress responsive phosphosites are slightly overlapped with those altered by the RCAR6 overexpression.

Figure S7. Proteomic profiles are altered in the RCAR overexpressing lines.

Figure S8. The proteins in wax metabolism and expansins are differentially accumulated in the RCAR6 overexpressing line.

Figure S9. The proteins in auxin and glucosinolate metabolism are differentially accumulated in the RCAR6 overexpressing line.

Figure S10. The proteins differentially expressed under drought stress conditions.

Figure S11. The metabolite profiles of the RCAR overexpressing lines are different from those of wild-type plants.

Figure S12. The primary metabolites altered in the RCAR overexpressing lines under well-watered and drought stress conditions.

Figure S13. Comparison of the diurnal changes of primary metabolites in the RCAR overexpressing lines.

Figure S14. Several primary metabolites are differentially accumulated in the RCAR overexpressing lines throughout the day.

Figure S15. The metabolism associated with photorespiration is unlikely to be changed in the RCAR overexpressing lines.

Figure S16. Different accumulation patterns are observed in several primary metabolites in the RCAR overexpressing lines.

Figure S17. The protein–protein interaction networks of the differentially phosphorylated proteins in the RCAR6 line.

Figure S18. The protein–protein interaction submodules of the differentially phosphorylated proteins in the RCAR6 line.

Figure S19. The protein–protein interaction networks of the differentially expressed proteins in the RCAR6 line.

Figure S20. The protein–protein interaction submodules of the differentially expressed proteins in the RCAR6 line.

Table S1. Differentially phosphorylated peptides in the RCAR6 overexpressing line.

Table S2. The phosphosites of the proteins in the GO term, protein phosphorylation showed increased phosphorylation in the RCAR6 overexpressing line.

Table S3. List of the differentially phosphorylated peptides in the RCAR6 overexpressing line found in SnRK2 and SnRK1 phosphoproteomic analyses.

Table S4. The phosphosites of the proteins in the GO term, chloroplast relocation, showed increased phosphorylation in the RCAR6 overexpressing line.

Table S5. The phosphosites of the proteins in the GO term, alternative mRNA splicing, showed increased phosphorylation in the RCAR6 overexpressing line.

Table S6. Differentially accumulated peptides in the RCAR6 overexpressing line.

REFERENCES

Altmann, M., **Altmann, S.**, **Rodriguez, P.A.**, **Weller, B.**, **Elorduy Vergara, L.**, **Palme, J.** ***et al.*** (2020) Extensive signal integration by the phytohormone protein network. *Nature*, **583**, 271–276.

Annunziata, M.G., **Apelt, F.**, **Carillo, P.**, **Krause, U.**, **Feil, R.**, **Koehl, K.** ***et al.*** (2018) Response of Arabidopsis primary metabolism and circadian clock to low night temperature in a natural light environment. *Journal of Experimental Botany*, **69**, 4881–4895.

Araújo, W.L., **Nunes-Nesi, A.**, **Osorio, S.**, **Usadel, B.**, **Fuentes, D.**, **Nagy, R.** ***et al.*** (2011) Antisense inhibition of the iron-sulphur subunit of succinate dehydrogenase enhances photosynthesis and growth in tomato via an organic acid-mediated effect on stomatal aperture. *Plant Cell*, **23**, 600–627.

Arenas-Huertero, F., **Arroyo, A.**, **Zhou, L.**, **Sheen, J.** & **León, P.** (2000) Analysis of Arabidopsis glucose insensitive mutants, gin5 and gin6, reveals a central role of the plant hormone ABA in the regulation of plant vegetative development by sugar. *Genes & Development*, **14**, 2085–2096.

Baena-González, E., **Rolland, F.**, **Thevelein, J.M.** & **Sheen, J.** (2007) A central integrator of transcription networks in plant stress and energy signalling. *Nature*, **448**, 938–942.

Belda-Palazón, B., **Adamo, M.**, **Valerio, C.**, **Ferreira, L.J.**, **Confraria, A.**, **Reis-Barata, D.** ***et al.*** (2020) A dual function of SnRK2 kinases in the regulation of SnRK1 and plant growth. *Nature Plants*, **6**, 1345–1353.

Belda-Palazón, B., **Costa, M.**, **Beeckman, T.**, **Rolland, F.** & **Baena-González, E.** (2022) ABA represses TOR and root meristem activity through nuclear exit of the SnRK1 kinase. *Proceedings of the National Academy of Sciences of the United States of America*, **119**, e2204862119.

Belda-Palazon, B., **Rodriguez, L.**, **Fernandez, M.A.**, **Castillo, M.C.**, **Anderson, E.M.**, **Gao, C.** ***et al.*** (2016) FYVE1/FREE1 interacts with the PYL4 ABA receptor and mediates its delivery to the vacuolar degradation pathway. *Plant Cell*, **28**, 2291–2311.

Belin, C., **de Franco, P.O.**, **Bourbousse, C.**, **Chaignepain, S.**, **Schmitter, J.M.**, **Vavasseur, A.** ***et al.*** (2006) Identification of features regulating OST1 kinase activity and OST1 function in guard cells. *Plant Physiology*, **141**, 1316–1327.

Boudsocq, M., **Droillard, M.J.**, **Barbier-Brygoo, H.** & **Laurière, C.** (2007) Different phosphorylation mechanisms are involved in the activation of sucrose non-fermenting 1 related protein kinases 2 by osmotic stresses and abscisic acid. *Plant Molecular Biology*, **63**, 491–503.

Bradford, M.M. (1976) A rapid and sensitive method for the quantitation of microgram quantities of protein utilizing the principle of protein-dye binding. *Analytical Biochemistry*, **72**, 248–254.

Broeckx, T., **Hulsmans, S.** & **Rolland, F.** (2016) The plant energy sensor: evolutionary conservation and divergence of SnRK1 structure, regulation, and function. *Journal of Experimental Botany*, **67**, 6215–6252.

Bueso, E., **Rodriguez, L.**, **Lorenzo-Orts, L.**, **Gonzalez-Guzman, M.**, **Sayas, E.**, **Muñoz-Bertomeu, J.** ***et al.*** (2014) The single-subunit RING-type E3 ubiquitin ligase RSL1 targets PYL4 and PYR1 ABA receptors in plasma membrane to modulate abscisic acid signaling. *The Plant Journal*, **80**, 1057–1071.

Caldana, C., **Li, Y.**, **Leisse, A.**, **Zhang, Y.**, **Bartholomaeus, L.**, **Fernie, A.R.** ***et al.*** (2013) Systemic analysis of inducible target of rapamycin mutants reveal a general metabolic switch controlling growth in *Arabidopsis thaliana*. *The Plant Journal*, **73**, 897–909.

Carianopol, C.S., **Chan, A.L.**, **Dong, S.**, **Provart, N.J.**, **Lumba, S.** & **Gazzarrini, S.** (2020) An abscisic acid-responsive protein interaction network for sucrose non-fermenting related kinase1 in abiotic stress response. *Communications Biology*, **3**, 145.

Carvalho, R.F., **Carvalho, S.D.** & **Duque, P.** (2010) The plant-specific SR45 protein negatively regulates glucose and ABA signaling during early seedling development in Arabidopsis. *Plant Physiology*, **154**, 772–783.

Carvalho, R.F., **Szakonyi, D.**, **Simpson, C.G.**, **Barbosa, I.C.**, **Brown, J.W.**, **Baena-González, E.** ***et al.*** (2016) The Arabidopsis SR45 splicing factor, a negative regulator of sugar signaling, modulates SNF1-related protein kinase 1 stability. *Plant Cell*, **28**, 1910–1925.

Cheng, A., **Grant, C.E.**, **Noble, W.S.** & **Bailey, T.L.** (2019) MoMo: discovery of statistically significant post-translational modification motifs. *Bioinformatics*, **35**, 2774–2782.

Cheng, C.Y., **Krishnakumar, V.**, **Chan, A.P.**, **Thibaud-Nissen, F.**, **Schobel, S.** & **Town, C.D.** (2017) Araport11: a complete reannotation of the *Arabidopsis thaliana* reference genome. *The Plant Journal*, **89**, 789–804.

Cho, H.-Y., **Wen, T.-N.**, **Wang, Y.-T.** & **Shih, M.-C.** (2016) Quantitative phosphoproteomics of protein kinase SnRK1 regulated protein phosphorylation in Arabidopsis under submergence. *Journal of Experimental Botany*, **67**, 2745–2760.

Clauw, P., **Coppens, F.**, **De Beuf, K.**, **Dhondt, S.**, **Van Daele, T.**, **Maleux, K.** ***et al.*** (2015) Leaf responses to mild drought stress in natural variants of *Arabidopsis thaliana*. *Plant Physiology*, **167**, 800–816.

Cutler, S.R., **Rodriguez, P.L.**, **Finkelstein, R.R.** & **Abrams, S.R.** (2010) Abscisic acid: emergence of a core signaling network. *Annual Review of Plant Biology*, **61**, 651–679.

Daloso, D.M., **Medeiros, D.B.**, **Dos Anjos, L.**, **Yoshida, T.**, **Araújo, W.L.** & **Fernie, A.R.** (2017) Metabolism within the specialized guard cells of plants. *The New Phytologist*, **216**, 1018–1033.

de Wit, M., **Galvão, V.C.** & **Fankhauser, C.** (2016) Light-mediated hormonal regulation of plant growth and development. *Annual Review of Plant Biology*, **67**, 513–537.

Deng, Z., **Oses-Prieto, J.A.**, **Kutschera, U.**, **Tseng, T.S.**, **Hao, L.**, **Burlingame, A.L.** ***et al.*** (2014) Blue light-induced proteomic changes in etiolated Arabidopsis seedlings. *Journal of Proteome Research*, **13**, 2524–2533.

Eckstein, A., **Krzeszowiec, W.**, **Banaś, A.K.**, **Janowiak, F.** & **Gabryś, H.** (2016) Abscisic acid and blue light signaling pathways in chloroplast movements in Arabidopsis mesophyll. *Acta Biochimica Polonica*, **63**, 449–458.

Endler, A., **Reiland, S.**, **Gerrits, B.**, **Schmidt, U.G.**, **Baginsky, S.** & **Martinoia, E.** (2009) In vivo phosphorylation sites of barley tonoplast proteins identified by a phosphoproteomic approach. *Proteomics*, **9**, 310–321.

Estruch, F., **Treitel, M.A.**, **Yang, X.** & **Carlson, M.** (1992) N-terminal mutations modulate yeast SNF1 protein kinase function. *Genetics*, **132**, 639–650.

Fernie, A.R., **Aharoni, A.**, **Willmitzer, L.**, **Stitt, M.**, **Tohge, T.**, **Kopka, J.** ***et al.*** (2011) Recommendations for reporting metabolite data. *Plant Cell*, **23**, 2477–2482.

Fujii, H. & **Zhu, J.K.** (2009) Arabidopsis mutant deficient in 3 abscisic acid-activated protein kinases reveals critical roles in growth, reproduction, and stress. *Proceedings of the National Academy of Sciences of the United States of America*, **106**, 8380–8385.

Fujita, Y., **Fujita, M.**, **Shinozaki, K.** & **Yamaguchi-Shinozaki, K.** (2011) ABA-mediated transcriptional regulation in response to osmotic stress in plants. *Journal of Plant Research*, **124**, 509–525.

Fujita, Y., **Nakashima, K.**, **Yoshida, T.**, **Katagiri, T.**, **Kidokoro, S.**, **Kanamori, N.** ***et al.*** (2009) Three SnRK2 protein kinases are the main positive regulators of abscisic acid signaling in response to water stress in Arabidopsis. *Plant & Cell Physiology*, **50**, 2123–2132.

Ge, S.X., **Jung, D.** & **Yao, R.** (2020) ShinyGO: a graphical gene-set enrichment tool for animals and plants. *Bioinformatics*, **36**, 2628–2629.

Gibon, Y., **Usadel, B.**, **Blaesing, O.E.**, **Kamlage, B.**, **Hoehne, M.**, **Trethewey, R.** ***et al.*** (2006) Integration of metabolite with transcript and enzyme activity profiling during diurnal cycles in Arabidopsis rosettes. *Genome Biology*, **7**, R76.

Gong, D., Guo, Y., Jagendorf, A.T. & Zhu, J.K. (2002) Biochemical characterization of the Arabidopsis protein kinase SOS2 that functions in salt tolerance. *Plant Physiology*, **130**, 256–264.

Gonzalez-Guzman, M., Pizzio, G.A., Antoni, R., Vera-Sirera, F., Merilo, E., Bassel, G.W. *et al.* (2012) Arabidopsis PYR/PYL/RCAR receptors play a major role in quantitative regulation of stomatal aperture and transcriptional response to abscisic acid. *Plant Cell*, **24**, 2483–2496.

Grondin, A., Rodrigues, O., Verdoucq, L., Merlot, S., Leonhardt, N. & Maurel, C. (2015) Aquaporins contribute to ABA-triggered stomatal closure through OST1-mediated phosphorylation. *Plant Cell*, **27**, 1945–1954.

Harb, A., Krishnan, A., Ambavaram, M.M. & Pereira, A. (2010) Molecular and physiological analysis of drought stress in Arabidopsis reveals early responses leading to acclimation in plant growth. *Plant Physiology*, **154**, 1254–1271.

Hawley, S.A., Davison, M., Woods, A., Davies, S.P., Beri, R.K., Carling, D. *et al.* (1996) Characterization of the AMP-activated protein kinase kinase from rat liver and identification of threonine 172 as the major site at which it phosphorylates AMP-activated protein kinase. *The Journal of Biological Chemistry*, **271**, 27879–27887.

Hoehenwarter, W., Thomas, M., Nukarinen, E., Egelhofer, V., Röhrig, H., Weckwerth, W. *et al.* (2013) Identification of novel in vivo MAP kinase substrates in *Arabidopsis thaliana* through use of tandem metal oxide affinity chromatography. *Molecular & Cellular Proteomics*, **12**, 369–380.

Hu, H., Boisson-Dernier, A., Israelsson-Nordström, M., Böhmer, M., Xue, S., Ries, A. *et al.* (2010) Carbonic anhydrases are upstream regulators of CO_2-controlled stomatal movements in guard cells. *Nature Cell Biology*, **12**, 87–93.

Inoue, S., Kinoshita, T., Matsumoto, M., Nakayama, K.I., Doi, M. & Shimazaki, K. (2008) Blue light-induced autophosphorylation of phototropin is a primary step for signaling. *Proceedings of the National Academy of Sciences of the United States of America*, **105**, 5626–5631.

Inoue, S.I. & Kinoshita, T. (2017) Blue light regulation of stomatal opening and the plasma membrane H(+)-ATPase. *Plant Physiology*, **174**, 531–538.

Jones, A.M., Xuan, Y., Xu, M., Wang, R.S., Ho, C.H., Lalonde, S. *et al.* (2014) Border control—a membrane-linked interactome of Arabidopsis. *Science*, **344**, 711–716.

Kamiyama, Y., Hirotani, M., Ishikawa, S., Minegishi, F., Katagiri, S., Rogan, C.J. *et al.* (2021) Arabidopsis group C Raf-like protein kinases negatively regulate abscisic acid signaling and are direct substrates of SnRK2. *Proceedings of the National Academy of Sciences of the United States of America*, **118**, e2100073118.

Komander, D. & Rape, M. (2012) The ubiquitin code. *Annual Review of Biochemistry*, **81**, 203–229.

Kopka, J., Schauer, N., Krueger, S., Birkemeyer, C., Usadel, B., Bergmüller, E. *et al.* (2005) GMD@CSB.DB: the Golm metabolome database. *Bioinformatics*, **21**, 1635–1638.

Laby, R.J., Kincaid, M.S., Kim, D. & Gibson, S.I. (2000) The Arabidopsis sugar-insensitive mutants sis4 and sis5 are defective in abscisic acid synthesis and response. *The Plant Journal*, **23**, 587–596.

Lee, S.C., Lan, W.Z., Kim, B.G., Li, L., Cheong, Y.H., Pandey, G.K. *et al.* (2007) A protein phosphorylation/dephosphorylation network regulates a plant potassium channel. *Proceedings of the National Academy of Sciences of the United States of America*, **104**, 15959–15964.

Léran, S., Edel, K.H., Pervent, M., Hashimoto, K., Corratgé-Faillie, C., Offenborn, J.N. *et al.* (2015) Nitrate sensing and uptake in Arabidopsis are enhanced by ABI2, a phosphatase inactivated by the stress hormone abscisic acid. *Science Signaling*, **8**, ra43.

Li, H., Li, Y., Zhao, Q., Li, T., Wei, J., Li, B. *et al.* (2019) The plant ESCRT component FREE1 shuttles to the nucleus to attenuate abscisic acid signalling. *Nature Plants*, **5**, 512–524.

Lisec, J., Schauer, N., Kopka, J., Willmitzer, L. & Fernie, A.R. (2006) Gas chromatography mass spectrometry-based metabolite profiling in plants. *Nature Protocols*, **1**, 387–396.

Liu, Y., Wang, F., Zhang, H., He, H., Ma, L. & Deng, X.W. (2008) Functional characterization of the Arabidopsis ubiquitin-specific protease gene family reveals specific role and redundancy of individual members in development. *The Plant Journal*, **55**, 844–856.

Ljung, K., Nemhauser, J.L. & Perata, P. (2015) New mechanistic links between sugar and hormone signalling networks. *Current Opinion in Plant Biology*, **25**, 130–137.

Luedemann, A., Strassburg, K., Erban, A. & Kopka, J. (2008) TagFinder for the quantitative analysis of gas chromatography—mass spectrometry (GC-MS)-based metabolite profiling experiments. *Bioinformatics*, **24**, 732–737.

Lumba, S., Cutler, S. & McCourt, P. (2010) Plant nuclear hormone receptors: a role for small molecules in protein-protein interactions. *Annual Review of Cell and Developmental Biology*, **26**, 445–469.

Ma, Y., Szostkiewicz, I., Korte, A., Moes, D., Yang, Y., Christmann, A. *et al.* (2009) Regulators of PP2C phosphatase activity function as abscisic acid sensors. *Science*, **324**, 1064–1068.

Mano, Y. & Nemoto, K. (2012) The pathway of auxin biosynthesis in plants. *Journal of Experimental Botany*, **63**, 2853–2872.

Mardia, K.V., Kent, J.T. & Bibby, J.M. (1979) *Multivariate analysis*. New York: Academic Press.

Mergner, J., Frejno, M., Messerer, M., Lang, D., Samaras, P., Wilhelm, M. *et al.* (2020) Proteomic and transcriptomic profiling of aerial organ development in Arabidopsis. *Scientific Data*, **7**, 334.

Mitreiter, S. & Gigolashvili, T. (2021) Regulation of glucosinolate biosynthesis. *Journal of Experimental Botany*, **72**, 70–91.

Mogami, J., Fujita, Y., Yoshida, T., Tsukiori, Y., Nakagami, H., Nomura, Y. *et al.* (2015) Two distinct families of protein kinases are required for plant growth under high external Mg2+ concentrations in Arabidopsis. *Plant Physiology*, **167**, 1039–1057.

Moreau, M., Azzopardi, M., Clément, G., Dobrenel, T., Marchive, C., Renne, C. *et al.* (2012) Mutations in the Arabidopsis homolog of LST8/GbetaL, a partner of the target of rapamycin kinase, impair plant growth, flowering, and metabolic adaptation to long days. *Plant Cell*, **24**, 463–481.

Nukarinen, E., Nägele, T., Pedrotti, L., Wurzinger, B., Mair, A., Landgraf, R. *et al.* (2016) Quantitative phosphoproteomics reveals the role of the AMPK plant ortholog SnRK1 as a metabolic master regulator under energy deprivation. *Scientific Reports*, **6**, 31697.

Nunes, C., Primavesi, L.F., Patel, M.K., Martinez-Barajas, E., Powers, S.J., Sagar, R. *et al.* (2013) Inhibition of SnRK1 by metabolites: tissue-dependent effects and cooperative inhibition by glucose 1-phosphate in combination with trehalose 6-phosphate. *Plant Physiology and Biochemistry*, **63**, 89–98.

Pandey, G.K., Cheong, Y.H., Kim, B.G., Grant, J.J., Li, L. & Luan, S. (2007) CIPK9: a calcium sensor-interacting protein kinase required for low-potassium tolerance in Arabidopsis. *Cell Research*, **17**, 411–421.

Park, S.Y., Fung, P., Nishimura, N., Jensen, D.R., Fujii, H., Zhao, Y. *et al.* (2009) Abscisic acid inhibits type 2C protein phosphatases via the PYR/PYL family of START proteins. *Science*, **324**, 1068–1071.

Pei, D., Hua, D., Deng, J., Wang, Z., Song, C., Wang, Y. *et al.* (2022) Phosphorylation of the plasma membrane H+-ATPase AHA2 by BAK1 is required for ABA-induced stomatal closure in Arabidopsis. *Plant Cell*, **34**, 2708–2729.

Raghavendra, A.S., Gonugunta, V.K., Christmann, A. & Grill, E. (2010) ABA perception and signalling. *Trends in Plant Science*, **15**, 395–401.

Reddy, A.S., Marquez, Y., Kalyna, M. & Barta, A. (2013) Complexity of the alternative splicing landscape in plants. *Plant Cell*, **25**, 3657–3683.

Ren, M., Venglat, P., Qiu, S., Feng, L., Cao, Y., Wang, E. *et al.* (2012) Target of rapamycin signaling regulates metabolism, growth, and life span in Arabidopsis. *Plant Cell*, **24**, 4850–4874.

Rodrigues, A., Adamo, M., Crozet, P., Margalha, L., Confraria, A., Martinho, C. *et al.* (2013) ABI1 and PP2CA phosphatases are negative regulators of Snf1-related protein kinase1 signaling in Arabidopsis. *Plant Cell*, **25**, 3871–3884.

Rook, F., Corke, F., Card, R., Munz, G., Smith, C. & Bevan, M.W. (2001) Impaired sucrose-induction mutants reveal the modulation of sugar-induced starch biosynthetic gene expression by abscisic acid signalling. *The Plant Journal*, **26**, 421–433.

Rubio, S., Rodrigues, A., Saez, A., Dizon, M.B., Galle, A., Kim, T.H. *et al.* (2009) Triple loss of function of protein phosphatases type 2C leads to partial constitutive response to endogenous abscisic acid. *Plant Physiology*, **150**, 1345–1355.

Ruprecht, B., Koch, H., Domasinska, P., Frejno, M., Kuster, B. & Lemeer, S. (2017) Optimized enrichment of phosphoproteomes by Fe-IMAC column chromatography. *Methods in Molecular Biology (Clifton, N.J.)*, **1550**, 47–60.

Ruprecht, B., Zecha, J., Zolg, D.P. & Kuster, B. (2017) High pH reversed-phase micro-columns for simple, sensitive, and efficient fractionation of

proteome and (TMT labeled) phosphoproteome digests. *Methods in Molecular Biology (Clifton, N.J.)*, **1550**, 83–98.

Schulze, W.X., **Schneider, T.**, **Starck, S.**, **Martinoia, E.** & **Trentmann, O.** (2012) Cold acclimation induces changes in Arabidopsis tonoplast protein abundance and activity and alters phosphorylation of tonoplast monosaccharide transporters. *The Plant Journal*, **69**, 529–541.

Schwartz, D. & **Gygi, S.P.** (2005) An iterative statistical approach to the identification of protein phosphorylation motifs from large-scale data sets. *Nature Biotechnology*, **23**, 1391–1398.

Selinski, J. & **Scheibe, R.** (2019) Malate valves: old shuttles with new perspectives. *Plant Biology (Stuttgart, Germany)*, **21**(Suppl 1), 21–30.

Shannon, P., **Markiel, A.**, **Ozier, O.**, **Baliga, N.S.**, **Wang, J.T.**, **Ramage, D.** ***et al.*** (2003) Cytoscape: a software environment for integrated models of biomolecular interaction networks. *Genome Research*, **13**, 2498–2504.

Singh, A., **Yadav, A.K.**, **Kaur, K.**, **Sanyal, S.K.**, **Jha, S.K.**, **Fernandes, J.L.** ***et al.*** (2018) A protein phosphatase 2C, AP2C1, interacts with and negatively regulates the function of CIPK9 under potassium-deficient conditions in Arabidopsis. *Journal of Experimental Botany*, **69**, 4003–4015.

Skelly, M.J., **Furniss, J.J.**, **Grey, H.**, **Wong, K.W.** & **Spoel, S.H.** (2019) Dynamic ubiquitination determines transcriptional activity of the plant immune coactivator NPR1. *eLife*, **8**, e47005.

Stenmark, H., **Aasland, R.**, **Toh, B.H.** & **D'Arrigo, A.** (1996) Endosomal localization of the autoantigen EEA1 is mediated by a zinc-binding FYVE finger. *The Journal of Biological Chemistry*, **271**, 24048–24054.

Sugden, C., **Donaghy, P.G.**, **Halford, N.G.** & **Hardie, D.G.** (1999) Two SNF1-related protein kinases from spinach leaf phosphorylate and inactivate 3-hydroxy-3-methylglutaryl-coenzyme A reductase, nitrate reductase, and sucrose phosphate synthase in vitro. *Plant Physiology*, **120**, 257–274.

Sullivan, S., **Thomson, C.E.**, **Lamont, D.J.**, **Jones, M.A.** & **Christie, J.M.** (2008) In vivo phosphorylation site mapping and functional characterization of Arabidopsis phototropin 1. *Molecular Plant*, **1**, 178–194.

Suzuki, H., **Koshiba, T.**, **Fujita, C.**, **Yamauchi, Y.**, **Kimura, T.**, **Isobe, T.** ***et al.*** (2019) Low-fluence blue light-induced phosphorylation of Zmphot1 mediates the first positive phototropism. *Journal of Experimental Botany*, **70**, 5929–5941.

Szklarczyk, D., **Gable, A.L.**, **Lyon, D.**, **Junge, A.**, **Wyder, S.**, **Huerta-Cepas, J.** ***et al.*** (2019) STRING v11: protein–protein association networks with increased coverage, supporting functional discovery in genome-wide experimental datasets. *Nucleic Acids Research*, **47**, D607–D613.

Tajdel, M., **Mituła, F.** & **Ludwików, A.** (2016) Regulation of Arabidopsis MAPKKK18 by ABI1 and SnRK2, components of the ABA signaling pathway. *Plant Signaling & Behavior*, **11**, e1139277.

Tischer, S.V., **Wunschel, C.**, **Papacek, M.**, **Kleigrewe, K.**, **Hofmann, T.**, **Christmann, A.** ***et al.*** (2017) Combinatorial interaction network of abscisic acid receptors and coreceptors from *Arabidopsis thaliana*. *Proceedings of the National Academy of Sciences of the United States of America*, **114**, 10280–10285.

Toroser, D., **Plaut, Z.** & **Huber, S.C.** (2000) Regulation of a plant SNF1-related protein kinase by glucose-6-phosphate. *Plant Physiology*, **123**, 403–412.

Tyanova, S., **Temu, T.** & **Cox, J.** (2016) The MaxQuant computational platform for mass spectrometry-based shotgun proteomics. *Nature Protocols*, **11**, 2301–2319.

Tyanova, S., **Temu, T.**, **Sinitcyn, P.**, **Carlson, A.**, **Hein, M.Y.**, **Geiger, T.** ***et al.*** (2016) The Perseus computational platform for comprehensive analysis of (prote)omics data. *Nature Methods*, **13**, 731–740.

Umezawa, T., **Sugiyama, N.**, **Takahashi, F.**, **Anderson, J.C.**, **Ishihama, Y.**, **Peck, S.C.** ***et al.*** (2013) Genetics and phosphoproteomics reveal a protein phosphorylation network in the abscisic acid signaling pathway in *Arabidopsis thaliana*. *Science Signaling*, **6**, rs8.

Urbanczyk-Wochniak, E., **Baxter, C.**, **Kolbe, A.**, **Kopka, J.**, **Sweetlove, L.J.** & **Fernie, A.R.** (2005) Profiling of diurnal patterns of metabolite and transcript abundance in potato (*Solanum tuberosum*) leaves. *Planta*, **221**, 891–903.

Valenzuela-Riffo, F., **Parra-Palma, C.**, **Ramos, P.** & **Morales-Quintana, L.** (2020) Molecular and structural insights into FaEXPA5, an alpha-expansin protein related with cell wall disassembly during ripening of strawberry fruit. *Plant Physiology and Biochemistry*, **154**, 581–589.

van Leeuwen, W., **Okrész, L.**, **Bögre, L.** & **Munnik, T.** (2004) Learning the lipid language of plant signalling. *Trends in Plant Science*, **9**, 378–384.

van Wijk, K.J., **Friso, G.**, **Walther, D.** & **Schulze, W.X.** (2014) Meta-analysis of *Arabidopsis thaliana* phospho-proteomics data reveals compartmentalization of phosphorylation motifs. *Plant Cell*, **26**, 2367–2389.

Vizcaíno, J.A., **Csordas, A.**, **Del-Toro, N.**, **Dianes, J.A.**, **Griss, J.**, **Lavidas, I.** ***et al.*** (2016) 2016 Update of the PRIDE database and its related tools. *Nucleic Acids Research*, **44**, D447–D456.

Vlad, F., **Rubio, S.**, **Rodrigues, A.**, **Sirichandra, C.**, **Belin, C.**, **Robert, N.** ***et al.*** (2009) Protein phosphatases 2C regulate the activation of the Snf1-related kinase OST1 by abscisic acid in Arabidopsis. *Plant Cell*, **21**, 3170–3184.

Waidmann, S., **Kusenda, B.**, **Mayerhofer, J.**, **Mechtler, K.** & **Jonak, C.** (2014) A DEK domain-containing protein modulates chromatin structure and function in Arabidopsis. *Plant Cell*, **26**, 4328–4344.

Wang, P., **Xue, L.**, **Batelli, G.**, **Lee, S.**, **Hou, Y.J.**, **Van Oosten, M.J.** ***et al.*** (2013) Quantitative phosphoproteomics identifies SnRK2 protein kinase substrates and reveals the effectors of abscisic acid action. *Proceedings of the National Academy of Sciences of the United States of America*, **110**, 11205–11210.

Wang, P., **Zhao, Y.**, **Li, Z.**, **Hsu, C.C.**, **Liu, X.**, **Fu, L.** ***et al.*** (2018) Reciprocal regulation of the TOR kinase and ABA receptor balances plant growth and stress response. *Molecular Cell*, **69**, 100–112.e6.

Whiteman, S.A., **Serazetdinova, L.**, **Jones, A.M.**, **Sanders, D.**, **Rathjen, J.**, **Peck, S.C.** ***et al.*** (2008) Identification of novel proteins and phosphorylation sites in a tonoplast enriched membrane fraction of *Arabidopsis thaliana*. *Proteomics*, **8**, 3536–3547.

Wingenter, K., **Schulz, A.**, **Wormit, A.**, **Wic, S.**, **Trentmann, O.**, **Hoermiller, I.I.** ***et al.*** (2010) Increased activity of the vacuolar monosaccharide transporter TMT1 alters cellular sugar partitioning, sugar signaling, and seed yield in Arabidopsis. *Plant Physiology*, **154**, 665–677.

Wingenter, K., **Trentmann, O.**, **Winschuh, I.**, **Hörmiller, I.I.**, **Heyer, A.G.**, **Reinders, J.** ***et al.*** (2011) A member of the mitogen-activated protein 3-kinase family is involved in the regulation of plant vacuolar glucose uptake. *The Plant Journal*, **68**, 890–900.

Witt, S., **Galicia, L.**, **Lisec, J.**, **Cairns, J.**, **Tiessen, A.**, **Araus, J.L.** ***et al.*** (2012) Metabolic and phenotypic responses of greenhouse-grown maize hybrids to experimentally controlled drought stress. *Molecular Plant*, **5**, 401–417.

Wu, Y., **Thorne, E.T.**, **Sharp, R.E.** & **Cosgrove, D.J.** (2001) Modification of expansin transcript levels in the maize primary root at low water potentials. *Plant Physiology*, **126**, 1471–1479.

Xiong, Y. & **Sheen, J.** (2014) The role of target of rapamycin signaling networks in plant growth and metabolism. *Plant Physiology*, **164**, 499–512.

Yan, J., **Wang, P.**, **Wang, B.**, **Hsu, C.C.**, **Tang, K.**, **Zhang, H.** ***et al.*** (2017) The SnRK2 kinases modulate miRNA accumulation in Arabidopsis. *PLoS Genetics*, **13**, e1006753.

Yang, Z., **Liu, J.**, **Poree, F.**, **Schaeufele, R.**, **Helmke, H.**, **Frackenpohl, J.** ***et al.*** (2019) Abscisic acid receptors and coreceptors modulate plant water use efficiency and water productivity. *Plant Physiology*, **180**, 1066–1080.

Yang, Z., **Liu, J.**, **Tischer, S.V.**, **Christmann, A.**, **Windisch, W.**, **Schnyder, H.** ***et al.*** (2016) Leveraging abscisic acid receptors for efficient water use in Arabidopsis. *Proceedings of the National Academy of Sciences of the United States of America*, **113**, 6791–6796.

Yoshida, T., **Christmann, A.**, **Yamaguchi-Shinozaki, K.**, **Grill, E.** & **Fernie, A.R.** (2019) Revisiting the basal role of ABA – roles outside of stress. *Trends in Plant Science*, **24**, 625–635.

Yoshida, T., **Obata, T.**, **Feil, R.**, **Lunn, J.E.**, **Fujita, Y.**, **Yamaguchi-Shinozaki, K.** ***et al.*** (2019) The role of Abscisic acid signaling in maintaining the metabolic balance required for Arabidopsis growth under nonstress conditions. *Plant Cell*, **31**, 84–105.

Zecha, J., **Satpathy, S.**, **Kanashova, T.**, **Avanessian, S.C.**, **Kane, M.H.**, **Clauser, K.R.** ***et al.*** (2019) TMT labeling for the masses: a robust and cost-efficient, in-solution labeling approach. *Molecular & Cellular Proteomics*, **18**, 1468–1478.

Zhang, Y., **Primavesi, L.F.**, **Jhurreea, D.**, **Andralojc, P.J.**, **Mitchell, R.A.**, **Powers, S.J.** ***et al.*** (2009) Inhibition of SNF1-related protein kinase1 activity and regulation of metabolic pathways by trehalose-6-phosphate. *Plant Physiology*, **149**, 1860–1871.

Zhao, J., **Zhou, H.**, **Zhang, M.**, **Gao, Y.**, **Li, L.**, **Gao, Y.** ***et al.*** (2016) Ubiquitin-specific protease 24 negatively regulates abscisic acid signalling in *Arabidopsis thaliana*. *Plant, Cell & Environment*, **39**, 427–440.

Zhao, M., **Han, Y.**, **Feng, Y.**, **Li, F.** & **Wang, W.** (2012) Expansins are involved in cell growth mediated by abscisic acid and indole-3-acetic acid under drought stress in wheat. *Plant Cell Reports*, **31**, 671–685.

Zhao, Y. (2018) Essential roles of local auxin biosynthesis in plant development and in adaptation to environmental changes. *Annual Review of Plant Biology*, **69**, 417–435.

Zhao, Y., **Chan, Z.**, **Gao, J.**, **Xing, L.**, **Cao, M.**, **Yu, C.** ***et al.*** (2016) ABA receptor PYL9 promotes drought resistance and leaf senescence. *Proceedings of the National Academy of Sciences of the United States of America*, **113**, 1949–1954.

Zhao, Y., **Zhang, Z.**, **Gao, J.**, **Wang, P.**, **Hu, T.**, **Wang, Z.** ***et al.*** (2018) Arabidopsis duodecuple mutant of PYL ABA receptors reveals PYL repression of ABA-independent SnRK2 activity. *Cell Reports*, **23**(11), 3340–3351.e5.